Biochimica et Biophysica Acta 1827 (2013) 1123–1139

Contents lists available at SciVerse ScienceDirect

Biochimica et Biophysica Acta

journal homepage: www.elsevier.com/locate/bbabio

Review

A modular, energy-based approach to the development of nickel containing molecular electrocatalysts for hydrogen production and oxidation ☆

Wendy J. Shaw, Monte L. Helm *, Daniel L. DuBois

Physical Sciences Division, Pacific Northwest National Laboratory, P.O. Box 999, K2-57, Richland, WA 99352, USA

ARTICLE INFO

Article history:
Received 26 September 2012
Received in revised form 26 December 2012
Accepted 4 January 2013
Available online 11 January 2013

Keywords:
Hydrogen
Electrochemistry
Hydrogenase mimic
Homogeneous catalysis
Proton transport

ABSTRACT

This review discusses the development of molecular electrocatalysts for H_2 production and oxidation based on nickel. A modular approach is used in which the structure of the catalyst is divided into first, second, and outer coordination spheres. The first coordination sphere consists of the ligands bound directly to the metal center, and this coordination sphere can be used to control such factors as the presence or absence of vacant coordination sites, redox potentials, hydride donor abilities and other important thermodynamic parameters. The second coordination sphere includes functional groups such as pendent acids or bases that can interact with bound substrates such as H_2 molecules and hydride ligands, but that do not form strong bonds with the metal center. These functional groups can play diverse roles such as assisting the heterolytic cleavage of H_2, controlling intra- and intermolecular proton transfer reactions, and providing a physical pathway for coupling proton and electron transfer reactions. By controlling both the hydride donor ability of the catalysts using the first coordination sphere and the proton donor abilities of the functional groups in the second coordination sphere, catalysts can be designed that are biased toward H_2 production, oxidation, or bidirectional (catalyzing both H_2 oxidation and production). The outer coordination sphere is defined as that portion of the catalytic system that is beyond the second coordination sphere. This coordination sphere can assist in the delivery of protons and electrons to and from the catalytically active site, thereby adding another important avenue for controlling catalytic activity. Many features of these simple catalytic systems are good models for enzymes, and these simple systems provide insights into enzyme function and reactivity that may be difficult to probe in enzymes. This article is part of a Special Issue entitled: Metals in Bioenergetics and Biomimetics Systems.

1. Introduction

Increased use of renewable energies such as wind and solar is important for reducing CO_2 emissions and ensuring a sustainable energy supply. The inherent intermittency of power generation from solar and wind coupled with the need for transportation fuels will require the large-scale storage of energy generated from renewable sources. Properly designed electrocatalysts offer the potential for highly efficient interconversion between electricity and fuels, avoiding much of the thermal energy loss observed in the combustion of fossil fuels. At times of high electrical energy production from sources such as wind or solar technologies, electrocatalysis provides an excellent means to store energy in chemical bonds through the production of fuels. Additionally, electrocatalysis can be used for the production of electricity through the oxidation of fuels at times of high electrical demand. The simplest fuel is hydrogen, which can be produced by the reduction of two protons with two electrons. Currently the most efficient electrolyzers and PEM fuel cells use platinum for interconversion of electricity and hydrogen. The discovery of hydrogenase enzymes that produce and oxidize hydrogen using active sites containing the earth-abundant metals iron and nickel has inspired scientists to pursue more abundant and less expensive alternatives to platinum [1].

Of the three types of hydrogenases, the bimetallic hydrogenases, containing either two iron atoms ([FeFe]-hydrogenases) or both a nickel and iron atom ([NiFe]-hydrogenases), produce and oxidize hydrogen. The active site of the [FeFe]-hydrogenase enzyme, shown in Fig. 1 with H_2, uses a pendent amine to assist in heterolytic cleavage or formation of H_2. In addition to the active site, the surrounding protein matrix is used to deliver electrons through an attached Fe_4S_4 cluster (Fig. 1). Precise delivery and removal of protons or H_2 to the active site is accomplished by structured channels formed by the protein tertiary structure.

Numerous structural models of the [FeFe]-hydrogenases have been synthesized [2–8], and many are functional in that they perform some of the same reactions as the natural hydrogenases. For example, the Pickett, Rauchfuss, Darensbourg, Gloaguen and Lichtenberger groups have all reported functional models of the hydrogenase enzyme that

☆ This article is part of a Special Issue entitled: Metals in Bioenergetics and Biomimetics Systems.

* Corresponding author. Tel.: +1 509 375 2331.
E-mail address: monte.helm@pnnl.gov (M.L. Helm).

0005-2728/$ – see front matter © 2013 Elsevier B.V. All rights reserved.
http://dx.doi.org/10.1016/j.bbabio.2013.01.003

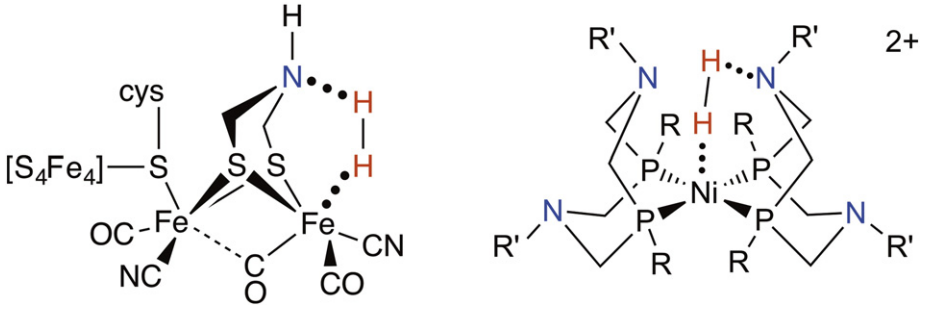

Fig. 1. [FeFe]-Hydrogenase active site (left) and $[Ni(P^{R}_{2}N^{R'}_{2})_2]^{2+}$ molecular catalyst (right), each with H_2 bound in the active site.

demonstrate electrocatalytic reduction of protons to form H_2 [9–13]. Several groups have also focused on the study of di-iron complexes containing azadithiolate ligands as structural models of the hydrogenase enzymes [2–5,14–16].

In contrast to *structural* models of [FeFe]-hydrogenase, our approach has been to design and probe biologically inspired *functional* models of hydrogenases [17–19]. The use of abundant, inexpensive metals and the incorporation of a pendent base adjacent to a vacant coordination site or hydride ligand are two critical components of the hydrogenase enzyme we sought to retain, without emulating the precise structural features exhibited by the [FeFe]-hydrogenases (Fig. 1). Our studies have shown that incorporation of positioned pendent amines can result in profound changes in reactivity, and the precise role of the pendent amine has been a primary focus of our research in developing nickel [17,20–24], cobalt [25–28], and iron catalysts for the electrocatalytic production and oxidation [29] of H_2. We have also begun investigating the role of the substrate delivery to the metal center beyond the pendent amine by exploring solvent effects [30] and attaching additional functional groups, such as amino acids [31–33], to the ligands of these well-defined molecular electrocatalysts. This review covers what has been learned using our modular, energy-based approach to molecular electrocatalysis. We will focus on nickel catalysts to illustrate the principles common to both enzymes and molecular catalysts.

2. Overview of design principles

The design of efficient electrocatalysts requires consideration of both structure and thermodynamics. Structural considerations entail careful design of ligand platforms to aid in the delivery of substrates to the metal center. Careful tailoring of ligand structure can also provide control over thermodynamic properties such as pK_a values and hydride donor abilities of metal hydride complexes. When the structure and thermodynamic properties are optimized, the result is a catalytic cycle that avoids large activation barriers and high or low energy intermediates that can hinder catalytic activity. Metalloproteins have evolved to result in optimized structural and thermodynamic properties, providing a biological source of inspiration for the development of synthetic molecular catalysts.

2.1. Modular structural approach

The structure of the $[Ni(P^{R}_{2}N^{R'}_{2})_2]^{2+}$ catalysts for hydrogen production/oxidation was developed using an approach modeled after metalloproteins. Metalloproteins can be described as containing unique regions or spheres which each contribute to catalysis. While they are sometimes split into only a first and second coordination sphere, for purposes of this review they will be defined more distinctly as the first, second, and outer coordination spheres (Fig. 2) [34]. The first coordination sphere consists of the ligands that are immediately attached to the metal(s). The second coordination sphere consists of functional groups incorporated into the ligand structure that preferentially interact with substrates and not the metal. An example is the interaction of the pendent amines with an entering H_2 molecule as shown in Fig. 1. The outer coordination sphere consists of the remainder of the protein scaffold, typically greater than ~3.5 to 4 Å from the metal [34].

2.1.1. First coordination sphere

The first coordination sphere influences the properties of the metal center such as the presence or absence of vacant coordination sites,

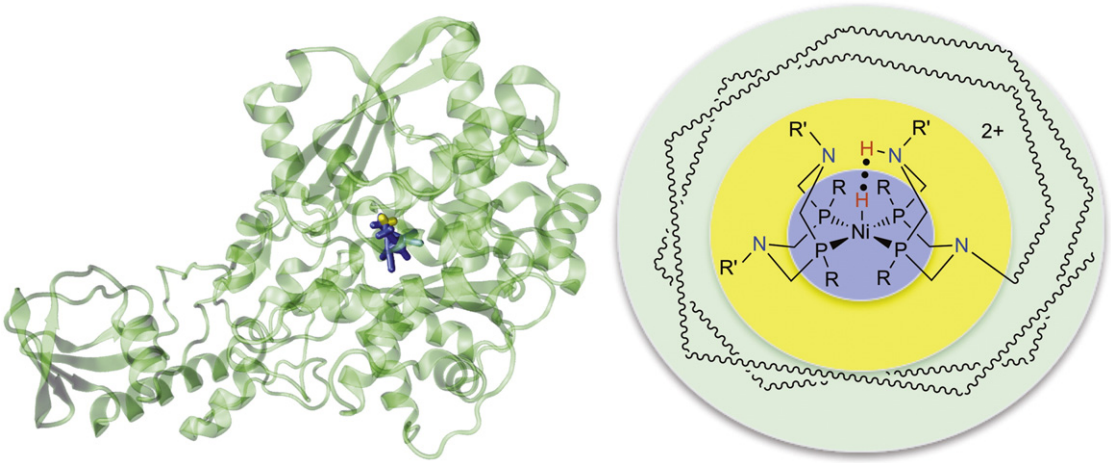

Fig. 2. Left, [FeFe]-hydrogenase (*Clostridium Pasteurianum*, PDB ID: 3C8Y) uses a first (blue), second (yellow), and outer (green ribbons) coordination sphere to control proton and electron movement. Right, our molecular catalysts mimic this approach by using a first coordination sphere (blue circle), which consists of the ligands immediately bound to the metal. The second coordination sphere (yellow circle) consists of functional groups that can interact with bound substrates but not directly bound to the metal. The outer coordination sphere (green) is anything outside of the first two spheres.

redox potentials, steric accessibility, and electron density. The cyanide and CO ligands in the active sites of hydrogenases are unusual for metalloenzymes. These ligands form strong bonds to transition metals in lower oxidation states, resulting in the formation of low-spin complexes. This feature is advantageous, because low spin complexes can result in vacant coordination sites that are required for interaction with H_2 to form hydride intermediates. Thus, nature's use of CN and CO ligands in the active site of hydrogenase can be understood in terms of ensuring a vacant coordination site on the metal center for H_2 binding.

For the $[Ni(P^R_2N^{R'}_2)_2]^{2+}$ catalysts shown in Figs. 1 and 2, the evolution of the first coordination sphere began with studies of low-spin $[M(diphosphine)_2]^{2+}$ and $[HM(diphosphine)_2]^{+}$ complexes (where M = Ni, Pd, and Pt) and an effort to relate the ligand structure to the pK_a values and hydride donor abilities of $[HM(diphosphine)_2]^{+}$ complexes. The pK_a values were found to depend solely on the electron donor abilities of the substituents on the diphosphine ligands, with larger pK_a values correlating to more electron donating substituents. Both experimental and theoretical studies show that there is a linear relationship between the potential of the M(I/0) couple of the $[M(diphosphine)_2]^{2+}$ complexes and the pK_a values of the corresponding $[HM(diphosphine)_2]^{+}$ complexes [35,36].

The free energy associated with heterolytic cleavage of an M–H bond of $[HM(diphosphine)_2]^{+}$ complexes to form a solvated hydride ligand and the corresponding metal complex (ΔG°_{H-}) exhibits a linear correlation with the M(II/I) couple of the corresponding $[M(diphosphine)_2]^{2+}$ complexes. The potential of the M(II/I) couples, and thus the ΔG°_{H-} values, are affected by two parameters; one parameter is the electron withdrawing or donating abilities of organic substituents on the diphosphine ligands, and the other parameter is the dihedral angle between the two chelating ligands, as shown in Fig. 3. This dihedral angle is largely controlled by steric interactions between substituents on the two diphosphine ligands. As the dihedral angle between the two diphosphine ligands increases for ligands with bulkier substituents or larger ring sizes, the tetrahedral distortion around the metal center also increases. As a result, the $[M(diphosphine)_2]^{2+}$ complex becomes a better hydride acceptor or the corresponding $[HM(diphosphine)_2]^{+}$ complex becomes a poorer hydride donor. This information regarding the factors controlling the acidity and hydride donor abilities of $[HM(diphosphine)_2]^{+}$ complexes is critical for the rational design of molecular electrocatalysts, as it results in the ability to help tune the catalysts for H_2 production, H_2 oxidation or bidirectional catalysis.

For $[Ni(diphosphine)_2]^{2+}$ complexes it was found that $[Ni(depp)_2]^{2+}$ (where depp is $Et_2PCH_2CH_2CH_2PEt_2$, Fig. 4) was a very good hydride acceptor and therefore capable of heterolytically cleaving H_2 in the presence of amines of moderate basicity [37]. This $[Ni(depp)_2]^{2+}$ complex therefore provided a platform for studying the effects of introducing pendent amines in the second coordination sphere as discussed in the next section.

2.1.2. Second coordination sphere, incorporation of pendent amines

The slow rate of catalytic H_2 oxidation by $[Ni(depp)_2]^{2+}$ in the presence of the exogenous base triethylamine coupled with the publication of the crystal structure of [FeFe]-hydrogenase suggested that a pendent amine in the second coordination sphere [38–40] could act as an intramolecular proton acceptor and the metal center as a hydride acceptor. The PNP ligand ($Et_2PCH_2N(Me)CH_2PEt_2$), in which the central methylene (CH_2) unit of depp is replaced with a methylamine group, was synthesized to introduce a pendent amine in the second coordination sphere (Fig. 4, $[Ni(PNP)_2]^{2+}$) [37,39,41]. Indeed, the synthesis of $[Ni(P^{Et}N^{Me}P^{Et})_2]^{2+}$ and its reaction with H_2 produced a complex in which H_2 was cleaved heterolytically to form a hydride and a protonated PNP ligand, $[HNi(PNHP)(PNP)]^{2+}$ with the metal center acting as the hydride acceptor and the pendent amine of one diphosphine ligand as a proton acceptor (Fig. 5). On the basis of DFT calculations, this heterolytic cleavage reaction is thought to proceed through an H_2 complex in which one of the six-membered rings containing the pendent amines has adopted a boat conformation resulting in the close approach of the pendent amine N to the bound H_2 complex [20]. Compared to $[Ni(depp)_2]^{2+}$, $[Ni(PNP)_2]^{2+}$ lowers the potential at which the catalyst operates by 650 mV. This large potential shift is attributed to the coupling of electron transfer and proton transfer steps upon oxidation of the nickel hydride intermediate, $[HNi(PNP)_2]^{+}$. During this oxidation, an electron is transferred to the electrode and a proton is transferred from the nickel to the N atom of the pendent amine. Although the $[Ni(PNP)_2]^{2+}$ is a catalyst capable of oxidizing H_2 at much more negative potentials (and therefore at a

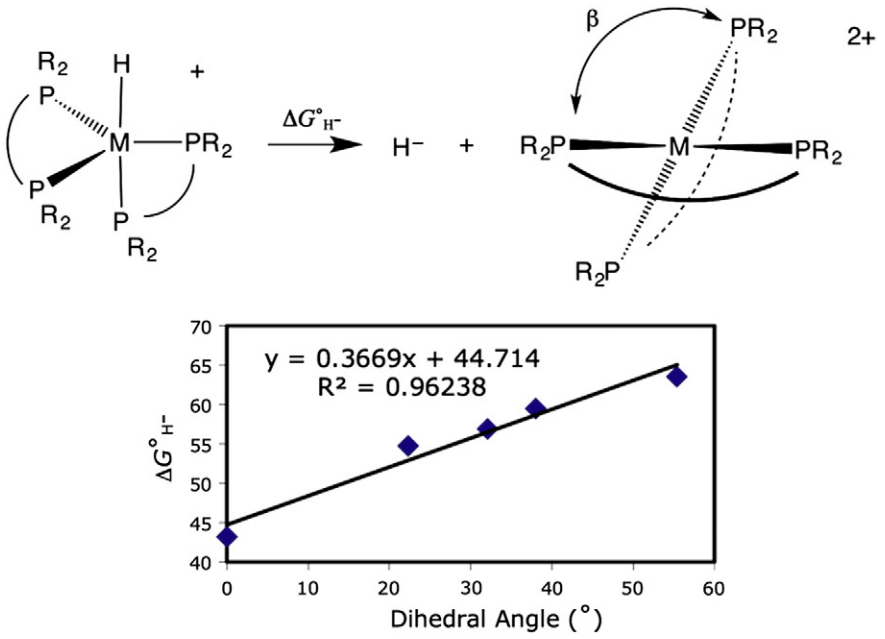

Fig. 3. Complexes containing M = Ni, Pd and Pt have been found to have a correlation between the dihedral angle (β) and the resulting hydricities of the metal (measured in CH_3CN).

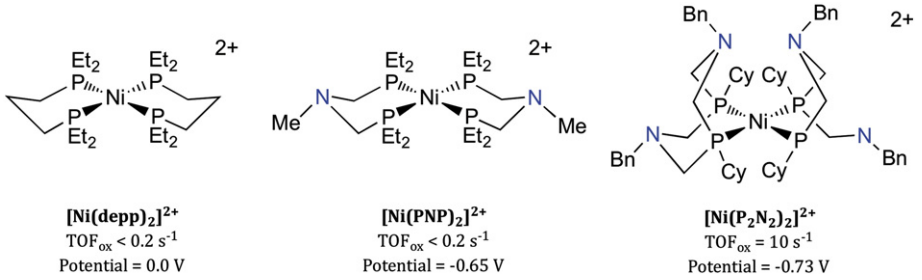

Fig. 4. The evolution of the second coordination sphere of the Ni-based hydrogen oxidation catalysts. Turnover frequencies and operating potentials (vs. $Cp_2Fe^{+/0}$) are shown.

lower overpotential) than the analogous $[Ni(depp)_2]^{2+}$ complex without the pendent amine, the turnover frequency (TOF) for this catalyst remains low, <0.2 s^{-1}.

2.1.3. Second coordination sphere, incorporation of positioned pendent amines

The six-membered rings of the $[Ni(PNP)_2]^{2+}$ undergo boat–chair interconversions (akin to those commonly observed for cyclohexyl rings), and thus the pendent amines are not positioned (i.e. held in close proximity to the vacant site of the metal center) as observed for the pendent amine in the [FeFe]-hydrogenase active site (see Fig. 1). In an effort to further enhance the rate of catalysis, $[Ni(P^R_2N^{R'}_2)_2]^{2+}$ complexes containing cyclic $P^R_2N^{R'}_2$ ligands were synthesized with the objective of forcing at least one six-membered ring of each diphosphine ligand to adopt a boat conformation and position a pendent amine in the immediate vicinity of the metal center (Fig. 4). It has been observed that $[Ni(P^R_2N^{R'}_2)_2]^{2+}$ complexes oxidize H_2 at rates at least two orders of magnitude faster than the $[Ni(PNP)_2]^{2+}$ complex that does not contain positioned pendent amines in its resting states [20]. The increased rates observed for the $[Ni(P^R_2N^{R'}_2)_2]^{2+}$ complexes have been attributed to the fact that their resting state includes a positioned pendent base that avoids the significant energy barrier associated with changing from a chair conformation to a boat conformation. Thus positioning of the pendent amine in close proximity to the metal center significantly enhances the rate of H_2 cleavage for these Ni complexes.

2.2. Outer coordination sphere

The outer coordination sphere found in proteins is not often studied in the context of molecular catalysts; however, the well-studied first and second coordination spheres of the $[Ni(P^R_2N^{R'}_2)_2]^{2+}$ catalyst system are ideally suited to a detailed study of functionalities incorporated into the outer coordination sphere. Solvent effects and the attachment of small functional groups such as amino acids and dipeptides on the periphery of these well-defined catalysts have been studied to determine the influence of the outer coordination sphere on catalysis. Our results, described in more detail below, demonstrate that the outer coordination sphere also has significant effects on catalytic properties such as turnover frequencies (TOFs) and overpotentials, indicating the importance of a properly designed outer coordination sphere for molecular catalysts.

3. Mechanistic studies of H_2 oxidation by $[Ni(P^R_2N^{R'}_2)_2]^{2+}$ complexes

The previous section describes some of the factors taken into account with the introduction of a pendent amine into the second coordination sphere, and the importance of positioning of the pendent amine in the immediate vicinity of the metal center to obtain high catalytic rates. In this section, mechanistic studies are described that shed further insight into the different roles the pendent amines play during catalysis. Although $[Ni(P^R_2N^{R'}_2)_2]^{2+}$ complexes for both hydrogen oxidation and production have been developed, more catalytic intermediates are observable for the hydrogen oxidation process, thus our mechanistic discussion emphasizes H_2 oxidation catalysts.

3.1. Mechanism of H_2 cleavage

As discussed above, $[Ni(PNP)_2]^{2+}$ cleaves H_2 heterolytically to form $HNi(PNHP)(PNP)]^{2+}$, a Ni(II) species in which the metal center has acted as a hydride acceptor and the pendent amine as a proton acceptor (Fig. 5). In contrast, the first intermediate observed upon reaction of $[Ni(P^R_2N^{R'}_2)_2]^{2+}$ complexes with H_2 is a Ni(0) species with two protonated pendent amines, as shown by structure **e/e**, short for endo/endo, since both protons are endo to the metal (Fig. 6, steps 1–2). In this complex, the two protons on the N atoms of the pendent amine also hydrogen bond to the Ni(0) center. As a result, both six-membered rings of the protonated amine ligands are in boat conformations and the protons are in endo positions with respect to the metal center. Although this endo/endo (**e/e**) complex is the first observable intermediate, theoretical calculations for $[Ni(P^{Cy}_2N^{Me}_2)_2]^{2+}$ (where Cy is cyclohexyl and Me is methyl) indicate that the cleavage of the H–H bond proceeds through a dihydrogen complex that evolves to an asymmetric transition state in which the Ni center interacts with one hydrogen atom and one pendent amine interacts with the other hydrogen of H_2 [42]. Cleavage of the H–H bond results in the formation of a nickel hydride intermediate with a protonated pendent amine in an endo position (**NiH/e** of Fig. 6, step 1). However, the barrier for proton transfer from Ni to a pendent amine of the unprotonated ligand is low (approximately 4 kcal/mol) and results in the immediate formation of the spectroscopically observed **e/e** species, $[Ni(P^{Cy}_2N^{Me}_2H)_2]^{2+}$. Theoretical calculations indicate a barrier for the overall process of hydrogen addition leading to the doubly protonated Ni(0) of 12–14 kcal/mol for $[Ni(P^{Cy}_2N^{Me}_2)_2]^{2+}$. Thus H_2

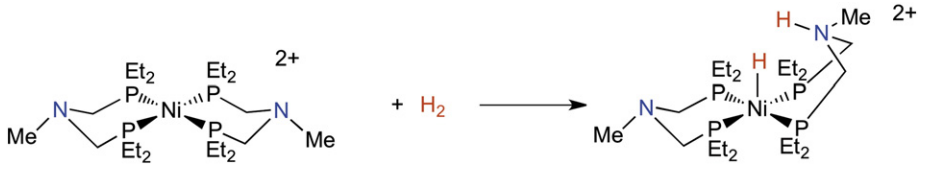

Fig. 5. Addition of H_2 to $[Ni(P^{Et}_2N^{Me}P^{Et}_2)_2]^{+2}$.

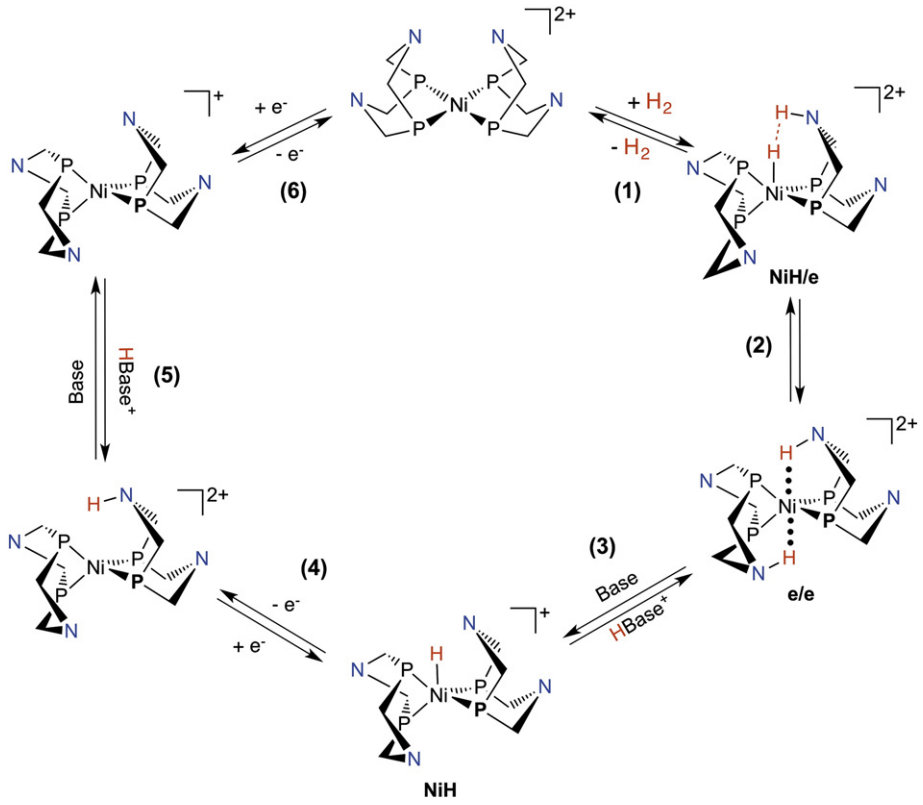

Fig. 6. The mechanism for hydrogen oxidation (clockwise) and hydrogen production (counter-clockwise). The R and R′ substituents on the phosphorus and nitrogen atoms, respectively, are omitted for clarity.

activation by $[Ni(P^{R}_2N^{R'}_2)_2]^{2+}$ complexes is thought to proceed through a two-center heterolytic cleavage of H_2, followed by intramolecular proton transfer from Ni to N (Fig. 6).

An alternative mechanism involving oxidative addition of H_2 to $[Ni(P^{Cy}_2N^{Me}_2)_2]^{2+}$ to form a Ni(IV) dihydride, $[(H)_2Ni(P^{Cy}_2N^{Me}_2)_2]^{2+}$, has also been characterized by computational studies [42]. This dihydride species is approximately 10 kcal/mol less stable than the **NiH/e** intermediate formed by heterolytic cleavage, and the barrier to its formation is 10–12 kcal/mol higher than that observed for the heterolytic cleavage reaction discussed in the previous paragraph. This would suggest that the dihydride species would not lie on the lowest energy catalytic pathway for the homoleptic $[Ni(P^{R}_2N^{R'}_2)_2]^{2+}$ complexes. However, addition of H_2 to the mixed ligand complex $[Ni(dppp)(P^{Ph}_2N^{Bn}_2)]^{2+}$ (where dppp is bis(diphenylphosphino)propane, Ph is phenyl, and Bn is benzyl) at −70 °C results in an equilibrium mixture of a dihydride species, $[(H)_2Ni(dppp)(P^{Ph}_2N^{Bn}_2)]^{2+}$, and a species in which both pendent amines of the $P^{Ph}_2N^{Bn}_2$ ligand are protonated, $[Ni(dppp)(P^{Ph}_2NH^{Bn}_2)]^{2+}$ (Fig. 7) [43]. In this case, the mechanism for formation of the $[(H)_2Ni(dppp)(P^{Ph}_2N^{Bn}_2)]^{2+}$ and $[Ni(dppp)(P^{Ph}_2NH^{Bn}_2)]^{2+}$ species is also thought to involve heterolytic cleavage to form a hydride with a protonated pendent amine, $[HNi(dppp)(P^{Ph}_2N^{Bn}NH^{Bn})]^{2+}$, followed by proton migration from N to Ni to form the dihydride species $[(H)_2Ni(dppp)(P^{Ph}_2N^{Bn}_2)]^{2+}$, or from Ni to N to form an **e/e** species with both protons on the same ligand, $[Ni(dppp)(P^{Ph}_2NH^{Bn}_2)]^{2+}$. More detailed theoretical calculations will be required to confirm the precise mechanism for this interesting system. In summary, when H_2 is added to either the homoleptic $[Ni(P^{R}_2N^{R'}_2)_2]^{2+}$ complexes or the heteroleptic $[Ni(dppp)(P^{Ph}_2N^{Bn}_2)]^{2+}$ complex, the mechanism for oxidation may go through different pathways that can be tuned by varying the ligand composition, but each of these pathways involve the pendent amine for H_2 cleavage.

3.2. Intramolecular proton exchange

For $[Ni(P^{Cy}_2N^{R}_2H)_2]^{2+}$ complexes with **e/e** geometries, the proton does not reside statically on the amine, but transfers quickly from N to Ni, resulting in a rapid intramolecular exchange of a proton between the two N atoms of the same diphosphine ligand, shown schematically in Fig. 8. This exchange has been observed and measured by $^{31}P\{^{1}H\}$ NMR spectroscopy [44]. For $[NiP^{Cy}_2N^{Bn}_2H)_2]^{2+}$ this exchange occurs with first order rate constants of 6000–12,000 s^{-1} at 298 K [44]. In addition to the transfer of a proton between the N atoms of the pendent amines, this exchange process also involves the movement of a hydride ligand from one face of the tetrahedron formed by the four P

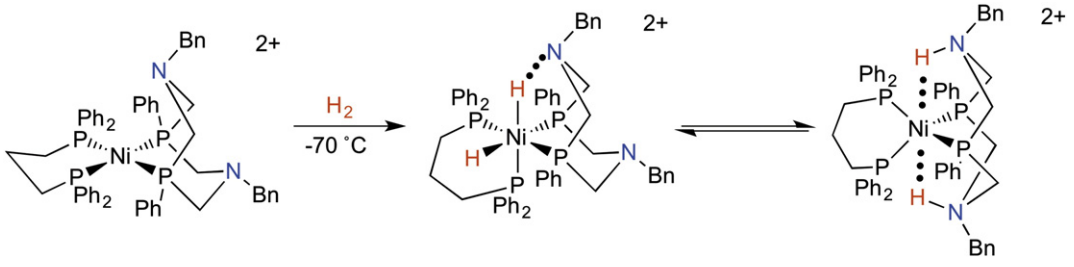

Fig. 7. Reaction of H_2 with a heteroleptic system produces different intermediates than homoleptics.

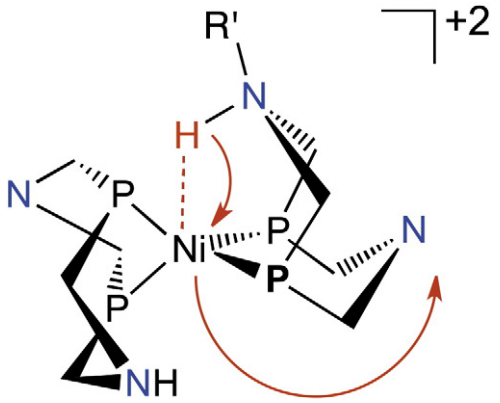

Fig. 8. Simplified schematic representation of the proton exchange mechanism for the endo/endo (**e/e**) isomer based on NMR and computational data. Red arrows indicate the metal-mediated proton movement between two nitrogens. Fig. 5 shows the complete mechanism for proton exchange.

atoms of the **NiH/e** (Fig. 8) intermediate to another (i.e. a fluxional hydride) and chair/boat interconversions of the two six-membered rings (Fig. 9). The chair/boat interconversion contributes most significantly to the barrier for this intramolecular exchange process. Thus when H_2 is added to $[Ni(P^R{}_2N^{R'}{}_2)_2]^{2+}$ the formation of the **e/e** species occurs via a heterolytic cleavage reaction followed by rapid and reversible proton transfer between the metal and the pendent amines. The result can be thought of as a cloud of protons distributed between the metal center and the ligands. For these Ni complexes this has the interesting consequence that *inter*molecular proton transfer, discussed in more detail below, could occur from any of the four pendent amines.

Similar rates are observed for the heteroleptic system mentioned above, where protonation of the Ni(0) complex, $Ni(dppp)(P^{Ph}{}_2N^{Bn}{}_2)$ leads to the formation of endo $[Ni(dppp)(P^{Ph}{}_2N^{Bn}N^{Bn}H)]^+$ in which protonation of a single pendent amine has occurred in an endo position. As with the homoleptic complex, rapid intramolecular exchange is seen for this complex, which involves the movement of the proton from one pendent amine to the other with an exchange rate exceeding $10^4\ s^{-1}$ at 10 °C, as observed with the homoleptic complexes. Addition of H_2 to the mixed ligand complex $[Ni(dppp)(P^{Ph}{}_2N^{Bn}{}_2)]^{2+}$ at −70 °C results in an equilibrium mixture of a dihydride species, $[(H)_2Ni(dppp)(P^{Ph}{}_2N^{Bn}{}_2)]^{2+}$, and a species in which both pendent amines of the $P^{Ph}{}_2N^{Bn}{}_2$ ligand are protonated, $[Ni(dppp)(P^{Ph}{}_2NH^{Bn}{}_2)]^{2+}$ (Fig. 7) [43]. Consistent with the facile proton transfer observed for this class of complex, these two species are in rapid equilibrium with each other, with an exchange rate between 10 and $100\ s^{-1}$ at −20 °C. These results are interpreted in terms of two sequential proton transfers between Ni and N involving $[(H)_2Ni(dppp)(P^{Ph}{}_2N^{Bn}{}_2)]^{2+}$, $[(H)Ni(dppp)(P^{Ph}{}_2N^{Bn}{}_2H)]^{2+}$, and $[Ni(dppp)(P^{Ph}{}_2N^{Bn}H_2)]^{2+}$. This intramolecular exchange of protons results in the rapid interconversion of Ni(0), Ni(II), and Ni(IV) species.

The fluxional nature of these Ni catalysts described above contrasts with the rigidity of the coordination environment around the distal iron of the [FeFe] hydrogenase. As a result, proton transfer to and from the distal iron occurs in the same direction that H_2 enters and leaves the active site. However, for the fluxional mononuclear Ni catalysts with pendent amines, proton transfer and H_2 binding and release are not required to occur in the same direction.

3.3. Intermolecular proton exchange and the presence of conformational isomers

In addition to the intramolecular proton exchange processes described in the preceding section, there are intermolecular exchange processes that occur in the presence of an exogenous base in solution. Irreversible deprotonation of the **e/e** species leads to the formation of the nickel(II) hydride (**NiH**) species as shown in Fig. 6, step 3. However, in the presence of weaker bases not capable of irreversible deprotonation, isomerization of the **e/e** species to form two new isomers with protons attached to the pendent amines in exo positions is observed (Fig. 10). For the endo/exo (**e/x**) isomer one proton remains in an endo position, as observed for the **e/e** isomer, and the other proton is in an exo position bridging two N atoms. Isomerization can continue so that both protons are positioned away from the Ni, as shown in Fig. 10 for the exo/exo (**x/x**) isomer, where both protons bridge the two N atoms of each ligand in an exo position. The structures of these three isomers have been confirmed by extensive ^1H, $^{31}P\{^1H\}$, and ^{15}N NMR studies for a variety of complexes with different $P^R{}_2N^{R'}{}_2$ ligands [21,44–46].

The rates of interconversion of the **e/e**, **e/x**, and **x/x** isomers depend strongly on the conditions and the isomers involved. In the absence of an exogenous base, the equilibration of the **e/e** and **e/x** isomers with the **x/x** isomer is slow, requiring days to reach equilibrium for complexes such as $[Ni(P^{Cy}{}_2N^{Bn}{}_2H)_2]^{2+}$ [47]. However, in the presence of

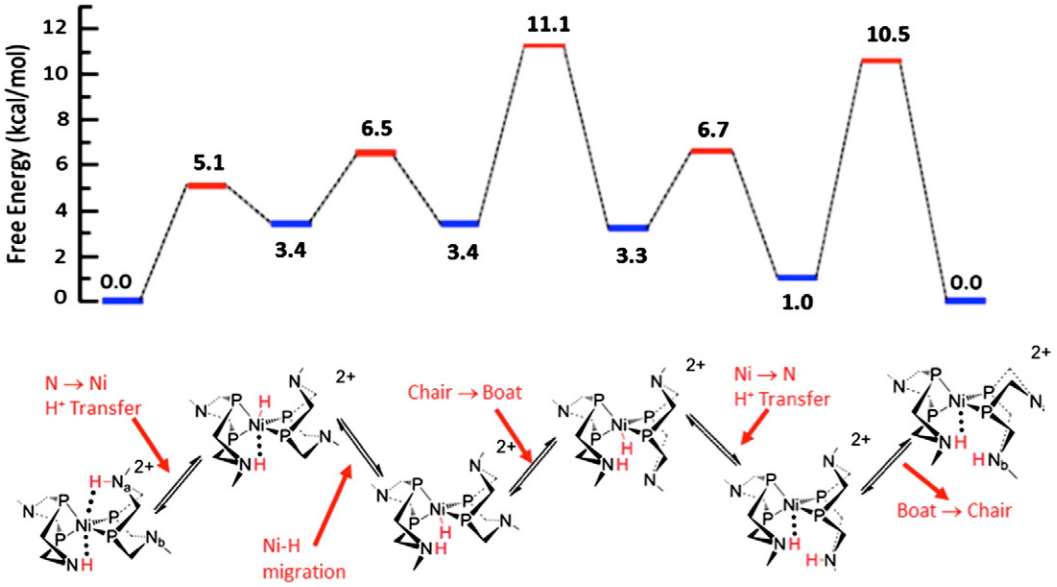

Fig. 9. Computational analysis of intramolecular proton transfer within the **e/e** $Ni(P^{Cy}{}_2N^{Me}{}_2H)_2$ complexes identifies the chair-to-boat isomerizations as the highest barriers.

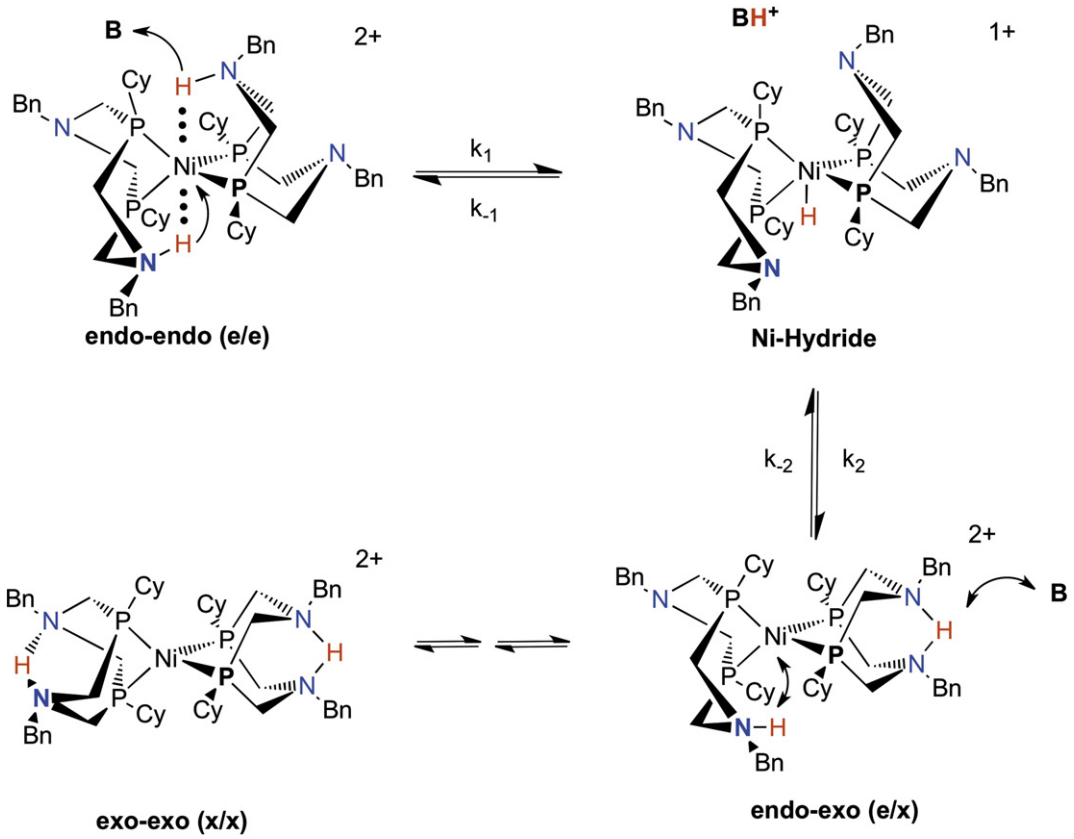

Fig. 10. Schematic representation of the base (B) catalyzed isomerization of the **e/e** species to the Ni-hydride, and to the other doubly protonated isomers with one proton (**e/x**) or two protons (**x/x**) positioned away from the metal.

a base such as aniline, this equilibration requires only a few minutes, with faster equilibration rates observed for bases with pK_a values close to that of the protonated pendent amine [47].

Compared to the rate of equilibration of the **e/e** and **e/x** isomers with the **x/x** isomer, the rate of equilibration of the **e/e** and **e/x** isomers is fast [47]. Detailed NMR studies of the interconversion of the **e/e** and **e/x** isomers of $[Ni(P^{Cy}_2N^{Bn}_2H)_2]^{2+}$ in conjunction with theoretical studies indicate that the mechanism of isomerization involves deprotonation at an endo or exo position to form a **NiH** intermediate followed by reprotonation at the other (i.e. exo or endo) position (Fig. 11) [47]. For $[Ni(P^{Cy}_2N^{Bn}_2H)_2]^{2+}$, the rate of protonation or deprotonation is rate limiting for interconversion, with the endo position being ~ an order of magnitude slower for both processes than for the exo position. These differences are attributed to differences in the accessibility of the endo and exo sites, as shown by the barriers calculated for the similar complex $[Ni(P^{Cy}_2N^{Me}_2H)_2]^{2+}$ in Fig. 11. Interactions between the acid or base in solution and the large cyclohexyl (Cy) group on P as the proton is removed from (or delivered to) the pendent amine endo to Ni result in larger barriers compared to the exo site.

For all complexes studied to date, the rate of interconversion of the **e/e** and **e/x** isomers is faster than the interconversion of **e/x** and **x/x** isomers. This is attributed to the greater stability of the **NiH** intermediate formed upon deprotonation of the **e/x** and **e/e** isomers compared to the **exo** intermediate formed by deprotonation of the **x/x** isomer in which the proton resides between two N atoms rather than on the Ni center. DFT calculations for the $[Ni(P^{Cy}_2N^{Me}_2)]^{2+}$ system indicate that the difference in stability of the **NiH** intermediate (~6.5 kcal/mol) and the protonated **exo** intermediate (~11.1 kcal/mol) is 4–5 kcal/mol, resulting in significantly different activation barriers [47].

As discussed above, the rates of isomer interconversion are enhanced in the presence of water. This enhancement may be due to water assisting in the cleavage of hydrogen bonds to Ni and N, water acting as a relay between the pendent amine and the exogenous base in solution, or both. These issues are currently under study. However, it is clear that the presence of these isomers is important. The larger activation barriers and slower rates for the interconversion of **x/x** and **e/x** isomers compared to the interconversion of **e/x** and **e/e** isomers suggest that the former isomerization process is more likely to be rate-determining than the later process. The barriers to these isomerization reactions are dependent on conditions, such as the identity of the exogenous base, that can result in barriers larger than those associated with H–H bond formation or H–H bond cleavage (Fig. 6). As a result, these isomers often play important roles during both H_2 oxidation and H_2 production catalysis as discussed in more detail below.

3.4. Themodynamic studies of the isomers in reduced and oxidized forms

The **e/e**, **e/x**, and **x/x** isomers are observed by NMR in significant quantities in equilibrium at room temperature [21], hence, these isomers are approximately equal in energy (within 1 kcal/mol of each other). However, the oxidation potentials of these three isomers differ significantly as shown in Fig. 12 [33] and Table 1 for several hydrogen oxidation catalysts [33,46,48]. This requires that the relative energies of the three Ni(I) isomers resulting from the oxidation of the **e/e**, **e/x**, and **x/x** isomers are significantly different. In the Ni(0) oxidation state, these isomers all have two hydrogen bonds, either Ni(0)•••H or N•••H. For the **e/e** isomer, two Ni(0)•••H hydrogen bonds are broken upon oxidation of Ni(0) to Ni(I). For the **e/x** isomer, one Ni(0)•••H bond is broken upon oxidation to Ni(I), and for the **x/x** isomer no Ni(0)•••H hydrogen bonds are broken upon oxidation. As a result, the **x/x** isomer is the easiest to oxidize (i.e. has the most negative redox potential), followed by the **e/x** isomer, and finally the **e/e** isomer. An alternate but equivalent explanation for the difference in

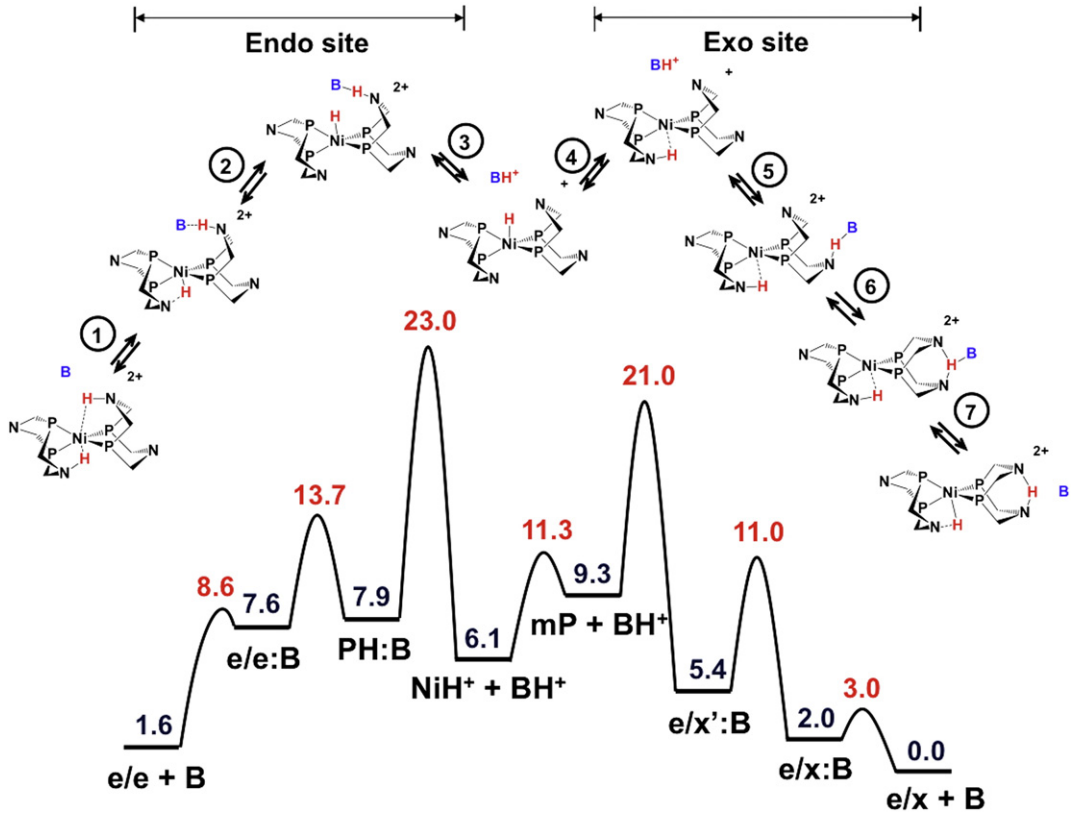

Fig. 11. The free energy diagram for $[Ni(P^{Cy}_2N^{Me}_2H)_2]^{2+}$ for the **e/e**⇆**e/x** isomerization mechanism catalyzed by aniline, **B**. The relative free energies with respect to **e/x** + **B** (in kcal/mol) of the various intermediates and the transition states are indicated with blue and red numbers, respectively. Reprinted with permission from O'Hagan, 2012, American Chemical Society [47].

redox potentials is that the Ni(0)•••H hydrogen bonds remove electron density from the Ni(0) center more effectively than N•••H hydrogen bonds. Thus the **e/e** isomer with two Ni(0)•••H hydrogen bonds is harder to oxidize than the **e/x** isomer with one Ni(0)•••H bond, which in turn is harder to oxidize than the **x/x** isomer with no Ni(0)•••H bonds [33,49].

The difference in the oxidation potentials of the **e/x** and **x/x** isomers corresponds to the Ni(0)•••H bond energy for the **e/x** isomer. For **e/x**-$[Ni(P^{tBu}_2N^{Bn}_2H)_2]^{2+}$, the Ni(0)•••H bond free energy is 7.4 kcal/mol [48]. The sum of the free energies of the two Ni(0)•••H hydrogen bonds in the **e/e** isomer is 11.3 kcal/mol. For a series of these complexes (Table 1), the difference in the oxidation potentials of the three isomers and hence the strength of these Ni(0)•••H bonds depends on the nature of the substituents on N, with a range of 6.3-9.5 kcal/mol for the **e/x** isomer. These differences reflect both steric interactions between the substituents on P and N as well as the electronic effects [33,48]. Theoretical calculations on the $[Ni(P^{Cy}_2N^{Me}_2H)_2]^{2+}$ complex indicate that the Ni(0)•••H hydrogen bonds and the N•••H hydrogen bonds are of roughly equal energy and comparable to those measured experimentally [42].

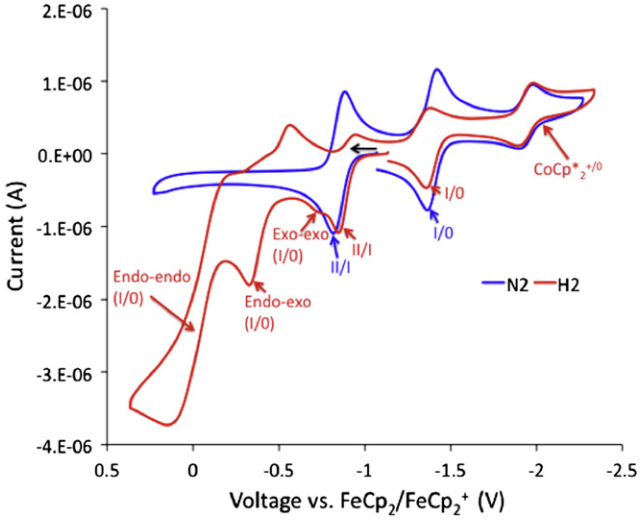

Fig. 12. Differences in the potentials between the endo–endo, endo–exo and exo–exo isomers, shown for $Ni(P^{Cy}_2N^{Bn\text{-}OMe}_2)_2$. Reprinted with permission from Lense, 2012, American Chemical Society [33].

In summary, the presence of intermolecular hydrogen bonding between a protonated pendent amine and the second pendent amine of the diphosphine ligand (an NH•••N bond) or between a protonated pendent amine and Ni(0) (an NH•••Ni(0) bond) results in the formation of stable isomers that can be observed spectroscopically and that have significantly different oxidation potentials. These hydrogen bonding interactions play major roles in determining the barriers to isomer interconversion and ultimately contribute to different catalytic pathways and hence the catalytic properties of these complexes.

3.5. Possible catalytic pathways following H – H bond cleavage

For $[Ni(P^R_2N^{R'}_2)_2]^{2+}$ complexes there are several possible pathways available to complete the catalytic cycle following the cleavage of the H – H bond and formation of the **e/e** isomer. The pathway observed depends on the particular catalyst and exogenous base under consideration. We will consider two general situations. In the first case, the base is sufficiently strong to irreversibly deprotonate the **e/e** isomer, preventing formation of the **e/x**, and **x/x** isomers. In the second case, a weaker base is used and deprotonation becomes reversible, resulting in formation of the **e/e**, **e/x**, and **x/x** isomers. However, in the latter case the exogenous base is sufficiently strong to irreversibly deprotonate the oxidized forms of the **e/e**, **e/x**, and **x/x** isomers (**e/e**$^+$, **e/x**$^+$, and **x/x**$^+$), which are thought to be significantly

Table 1
Reduction potentials for doubly protonated $[Ni(P^R_2N^{R'}H_2)_2]^{2+}$ isomers as well as the non-protonated $[Ni(P^R_2N^{R'}_2)_2]^{2+}$ (II/I) potentials.

$P^R_2N^{R'}_2$	e/e (V)	e/x (V)	x/x (V)	II/I (V)	Δ(e/e-e/x) (mV)	Δ(e/x-x/x) (mV)	Δ(II/I-e/e) (mV)
R = Cy R′ = $CH_2C_6H_4COOMe$	0.01	−0.24	−0.59	−0.74	250	350	750
R = Cy R′ = $CH_2C_6H_4OMe$	−0.04	−0.33	−0.74	−0.85	290	410	810
R = Cy R′ = ^{t}Bu	−0.36	−0.48	−0.75	−0.77	120	270	410
R = ^{t}Bu R′ = Bn	−0.12	−0.29	−0.61	−0.02	170	320	−100

more acidic than their reduced parents due to the increased positive charge. [33,49].

An example of catalysis in the presence of a strong base is the oxidation of H_2 using $[Ni(P^{Cy}_2N^{tBu}_2)_2]^+$ as the catalyst and triethylamine or *n*-butylamine as the base (Fig. 13) [46]. The pK_a values of the **e/e** (15.6), **e/x** (16.1), and **x/x** (16.5) isomers are significantly less than those of triethylamine (18.8) and *n*-butylamine (18.1). When the less bulky *n*-butylamine is used as the base, access to the endo proton is facile and deprotonation occurs rapidly from the **e/e** isomer to form the **NiH** intermediate, which is then followed by oxidation (Fig. 6, steps 3–4). In this case, the observed half-wave potential of the catalytic wave corresponds to that of the Ni(I/II) couple for $[Ni(P^{Cy}_2N^{tBu}_2)_2]^{+/2+}$ (Fig. 13, −0.77 V vs $Cp_2Fe^{+/0}$), due to the coupling of proton and electron transfer reactions for $[HNi(P^{Cy}_2N^{tBu}_2)_2]^+$ as discussed in more detail below.

When a large excess of triethylamine is used as the base, the *predominant* catalytic pathway is different, it first involves the oxidation of the **e/e** isomer (Fig. 13, −0.36 V vs $Cp_2Fe^{+/0}$) which is then followed by deprotonation. In this case, the steric bulk of triethylamine prevents facile access to the protons on the pendent amines of the **e/e** isomer. Once the **e/e** isomer is oxidized, the hydrogen bond between the Ni and the endo proton is broken due to the increased acidity of the Ni, and the distance between the protoned pendent amine and Ni increases. As a result, deprotonation becomes both thermodynamically and sterically more favorable, allowing catalysis to proceed.

The consequence of the above observations is that very different potentials are required for H_2 oxidation depending on the base used. For acetonitrile solutions containing sterically small strong bases, deprotonation occurs first and the catalytic oxidation of H_2 is observed at the II/I couple. For acetonitrile solutions containing sterically large strong bases, oxidation of the **e/e** isomer occurs more easily than deprotonation, resulting in the predominate catalytic pathway occurring at more positive potentials (~0.4 to 0.8 V, Table 1). Thus the ability of different sized bases to rapidly remove an endo proton results in large potential differences due to a change in the predominant catalytic pathway that is observed.

In the case of large amounts of weaker bases, however, deprotonation of the **e/e**, **e/x**, and **x/x** isomers is reversible. As an example, $[Ni(P^{Cy}_2N^{BnOMe}_2)_2]^{2+}$ catalyzes the oxidation of H_2 in the presence of large amounts of water (in this case the weak base) in acetonitrile [33]. For this catalytic system, water functions as a small base and equilibration of the **e/e** and **e/x** isomers is rapid compared to the rate of H_2 activation. As a result, H_2 oxidation occurs at the potential of the **e/x** isomer, which is more easily oxidized than the **e/e** isomer with which it is in equilibrium. In summary, the catalytic rate for this reaction is determined by the rate of the reaction of H_2 with $[Ni(P^{Cy}_2N^{BnOMe}_2)_2]^{2+}$ to form the **e/e** isomer, which is generally true for most $[Ni(P^R_2N^{R'}_2)_2]^{2+}$ H_2 oxidation catalysts. The potential at which the catalytic reaction occurs (and thus the overpotential) depends on the steric properties and strength of the exogenous base and the oxidation potentials of the **NiH**, **e/e**, and **e/x** intermediates.

3.6. Oxidation of catalytic intermediates and PCET

As discussed above, in the presence of a small strong base, the **e/e** isomer is deprotonated irreversibly to form the **NiH** intermediate. Oxidation of this hydride is then necessary to complete a catalytic cycle for H_2 oxidation (Fig. 6, step 4). In previous studies of $[HNi(diphosphine)_2]^+$ complexes, theoretical models were developed that allow us to accurately estimate the oxidation potentials of the NiH(III/II) couple, $E°$(III/II), for these non-pendent amine complexes using Eq. (1), where $E°$(I/0) is the redox potential of the $[Ni(diphosphine)_2]^{+/0}$ couple vs. the ferrocenium/ferrocene couple [8].

$$E°(III/II) = 1.02E°(I/0) + 1.60 \quad (1)$$

In trying to extend this relationship to the $[Ni(P^R_2N^{R'}_2)_2]^{2+}$ systems, something surprising is observed. For $[Ni(P^{tBu}_2N^{Bn}_2)_2]^{2+}$, the $E°$(I/0) couple is observed at −1.03 V, which would lead to the expectation that $[HNi(P^{tBu}_2N^{Bn}_2)_2]^+$ would oxidize at +0.55 V. The observed oxidation, however, occurs at −0.67 V, or 1.22 V more negative than expected. This large shift in potential arises from the coupling of the oxidation of this hydride, which involves an electron transfer to the electrode, and an intramolecular proton transfer from the Ni center to the pendent amine (Fig. 6, step 4). This is an intramolecular proton-coupled electron transfer reaction (PCET) and the observed potential shift is significantly larger for both $[HNi(PNP)_2]^+$ and $[HNi(P^R_2N^{R'}_2)_2]^+$ complexes compared to $[HNi(depp)_2]^+$, which requires an exogenous base such as NEt_3.

Mechanistically, such a PCET could occur by transferring a proton first followed by an electron transfer (PT–ET), by an electron transfer followed by a proton transfer (ET–PT), or by a process in which the

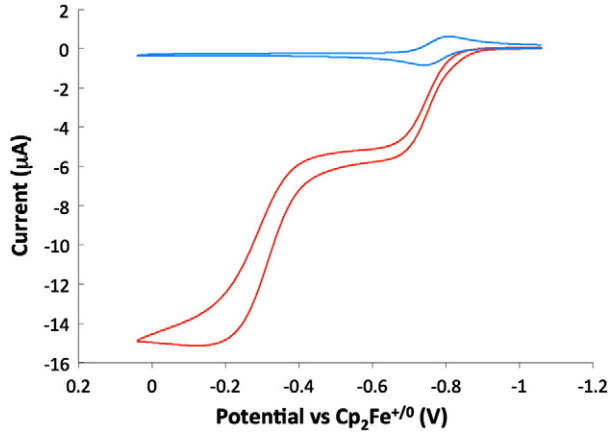

Fig. 13. Catalysis in the presence of strong bases such as NEt_3 occurs at two potentials: corresponding to the Ni(II/I) couple (−0.77 V), but predominantly at the couple of the e/e isomer, in this case, ≈−0.35 V.

electron and proton are transferred in a concerted process (EPT). Theoretical calculations for the $[HNi(P^{Me}_2N^{Me}_2)_2]^+$ and $[HNi(P^{Ph}_2N^{Bn}_2)_2]^+$ complexes suggest that the reactions proceed through an ET–PT process in most cases [50]. However, there may be exceptions to this general rule. For example, for the mixed-ligand complex [Ni(dppp)$(P^{Ph}_2N^{Bn}_2H)]^+$, the most stable form is not the hydride isomer with the hydrogen bound directly to Ni, but the isomer in which a proton is bound to N [43]. In cases such as this, the mechanism undoubtedly proceeds through a protonated N species that would be formed in the PT–ET mechanism of **NiH** intermediates. Thus whether a PT–ET or ET–PT pathway is followed depends on the particular catalyst being studied.

A second interesting feature of the theoretical studies is the suggestion that the mechanism for electron and proton transfer could become concerted if the N and Ni could approach each other more closely [50,51]. A closer approach is prevented by strain introduced into the six-membered ring as the N atom approaches Ni, and a more flexible pendent amine that is not constrained within a ring could possibly undergo a concerted reaction [52]. This possibility is under investigation.

In summary, experimental and theoretical studies indicate that oxidation of the **NiH** intermediate formed during the catalytic oxidation of H_2 involves the coupling of intramolecular proton transfer with an electron transfer reaction to the electrode. This reaction may proceed by either PT–ET or ET–PT transfer pathways depending on the particular catalyst involved, and may become concerted if more flexible proton relays can achieve a closer approach to the Ni center [52].

3.7. Final proton transfer and intermolecular PCET steps in the mechanism of hydrogen oxidation

The last two steps in the catalytic oxidation of H_2 involve the oxidation of the *endo*-$[Ni(P^R_2N^{R'}_2)(P^R_2N^{R'}_2H)]^{2+}$ species and proton transfer from the protonated pendent amine to a base in solution, an intermolecular proton transfer reaction (Fig. 6, steps 5–6). It has been experimentally observed that the oxidation potential of $[HNi(PNP)_2]^+$ shifts in the presence of an exogenous base [37]. As discussed above, this oxidation results in an intramolecular proton transfer from Ni to N to form the Ni(I) species with a protonated pendent amine, [Ni(PNP)$(PNHP)]^{2+}$. An exogenous base should not affect this intramolecular reaction. However, the coupling of an intermolecular proton transfer from the protonated pendent amine of $[Ni(PNP)(PNHP)]^{2+}$ to a base in solution with an electron transfer to the electrode would be expected to produce a potential shift as observed. It is expected that a similar process is occurring for the $[Ni(P^R_2N^{R'}_2)_2]^{2+}$ complexes and this intermolecular PCET process is currently under theoretical and experimental investigation. In summary, these intra- and intermolecular PCET reactions play a dramatic role in reducing the overpotentials of these catalysts, but they do not determine the rates of catalytic H_2 oxidation.

3.8. Hydrogen oxidation catalyst stability with respect to CO poisoning

Before leaving the topic of H_2 oxidation, it should be pointed out that these $[Ni(P^R_2N^{R'}_2)_2]^{2+}$ catalysts are not inhibited by CO, in contrast to Pt and many hydrogenase enzymes. Because CO is a frequent contaminant in H_2, and Pt fuel cells can be poisoned by CO even at the ppm level, the ability of CO to inhibit catalyst performance is an important consideration. The $[Ni(P^R_2N^{R'}_2)_2]^{2+}$ H_2 oxidation catalysts do react with CO to form five-coordinate complexes that have been characterized by X-ray crystallography [53]. However, CO binding is much weaker than H_2 binding, and consequently H_2 oxidation is not inhibited by concentrations of CO as high as 50% [20,43,53]. The preferential binding of H_2 over CO is attributed to the observation that the pendent amines interact much more strongly with the protons resulting from H_2 cleavage than they do with coordinated CO.

4. Catalytic H_2 production

4.1. Mechanistic considerations

The mechanism for the catalytic production of H_2 is essentially the reverse of that observed for H_2 oxidation (Fig. 6, counter-clockwise). Thus reduction of Ni(II) complexes to Ni(I) in acidic acetonitrile solutions is followed by protonation of a pendent amine to form $[Ni(P^R_2N^{R'}_2)(P^R_2N^{R'}_2H)]^{2+}$. This protonation step may occur at either an endo or exo position. Because of the paramagnetic nature of Ni(I) complexes, NMR studies to determine the precise position are not possible. However, detailed NMR studies of the protonation of the Ni(II) complex, $[Ni(P^{Ph}_2N^{Bn}_2)_2]^{2+}$, and the Ni(0) complexes, $Ni(P^{Ph}_2N^{Bn}_2)_2$ and $Ni(P^{Cy}_2N^{Bn}_2)_2$, indicate that protonation occurs with greater than 95% selectivity at the exo position (Fig. 14) [44,50,54]. Similarly, protonation of the hydride species, $[HNi(P^{Cy}_2N^{Bn}_2)_2]^+$, an intermediate in the proposed catalytic cycle (Fig. 6), also occurs in the exo position to form the **e/x** isomer in which the hydride proton has transferred to a N in the endo position [47]. These results, along with detailed theoretical studies, indicate that during the catalytic cycle, the kinetic product formed upon reduction and protonation of the catalyst is not the **e/e** isomer but the **x/x** isomer.

Because only the **e/e** isomer can evolve to eliminate H_2, as shown in Fig. 6, this represents a kinetic bottleneck for these catalysts. Thus the rate-determining step for the catalytic production of H_2 is not the formation of the H – H bond as shown in Fig. 14 (going counterclockwise around the cycle), but the deprotonation and protonation steps discussed above for the interconversion of the **x/x**, **e/x**, and **e/e** isomers. Also, as discussed above, the size of the acid used for the catalytic reaction and water affect the rate of interconversion of these isomers. As a result, the fastest catalytic rates for H_2 production are observed for small acids, and the addition of water produces significant enhancements in the catalytic rates [22,31]. This is illustrated by data for the $[Ni(P^{Ph}_2N^{Ph}_2)_2]^{2+}$ complex which has a turnover frequency of 31 s^{-1} when the bulky 2,6-dichloroanilinium (pK_a = 5.0 in acetonitrile) is used as an acid, 590 s^{-1} when the much smaller protonated dimethylformamide (pK_a = 6.1 in acetonitrile) is the acid, and even higher rates when water is added to catalytic solutions of these acids, 160 s^{-1} and 720 s^{-1} for 2,6-dichloroanilinium and protonated dimethylformamide, respectively [22]. Computational studies indicate that for all acids studied, the barrier for H_2 formation for $[Ni(P^{Ph}_2N^{Ph}_2)_2]^{2+}$ is dominated by the isomerization of the **x/x** to the **e/e** isomer and not the elimination of H_2 from the **e/e** species [42,47].

4.2. Thermodynamic considerations and tuning catalytic activity

The thermodynamic driving force for the addition of H_2 to $[Ni(P^R_2N^{R'}_2)_2]^{2+}$ catalysts can be calculated, as shown in Fig. 15, by measuring their $\Delta G°_{H-}$ and pK_a values. As discussed in the first coordination sphere Section (2.1.1), the electron donor abilities and steric properties of the substituents on P can be used to control the hydride donor/acceptor ability of these complexes (first equation in Fig. 15). The hydride acceptor abilities and pK_a values have been measured for a number of complexes of this class of compounds (first and second equations) [20,23,24,33,55–57], and the constant for the heterolytic cleavage of H_2 in acetonitrile (third equation) was taken from the literature [57]. Using these values and the equations in Fig. 15, the internal driving force for hydrogen production or oxidation for each individual catalyst can be calculated.

As seen from the equations in Fig. 15, changing the hydride acceptor ability and the amine pK_a values allows the catalytic driving force to be tuned. While the hydride acceptor ability of $[Ni(P^R_2N^{R'}_2)_2]^{2+}$ increases as the electron donor ability of the substituents on P decrease and as the steric bulk of the substituents increase, in practice the limitation on the hydride acceptor ability is the size of the substituents on P. The largest substituent on P that is compatible with the

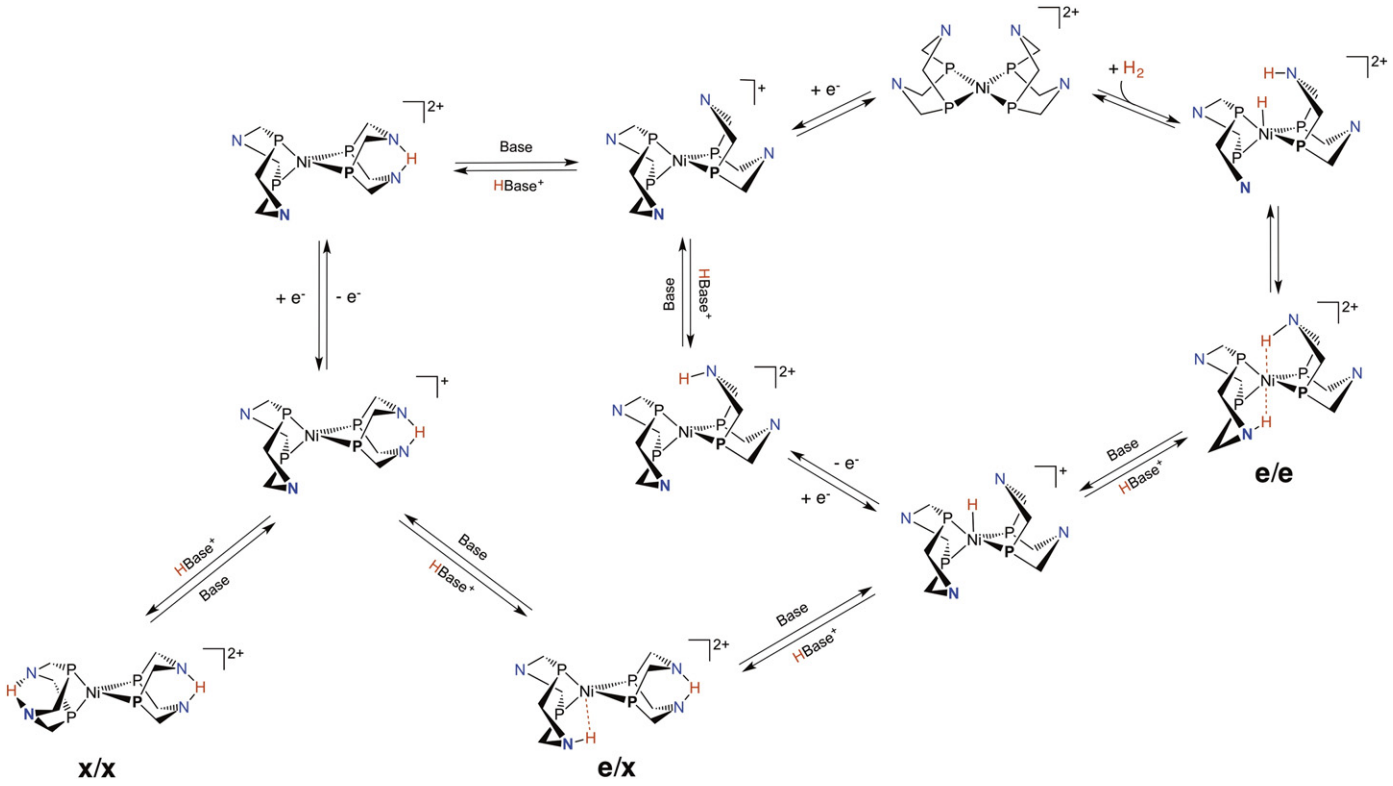

Fig. 14. The kinetic preference for exo protonation (top left) creates additional steps in the ideal catalytic cycle (circle), slowing the overall rate (R and R′ substituents on the phosphorus and nitrogen atoms are omitted for clarity). Reprinted with permission from O'Hagan, 2012, American Chemical Society [47].

coordination of two $P^{R}{}_{2}N^{R'}{}_{2}$ ligands is cyclohexyl. Complexes with cyclohexyl substituents on P have hydride acceptor abilities of approximately −61 kcal/mol. For example the hydride acceptor abilities of $[Ni(P^{R}{}_{2}N^{R'}{}_{2})_2]^{2+}$ are −61 kcal/mol for both R = Cy and R′ = Bn or *t*Bu [46,55]. In contrast, the hydride acceptor ability of $[Ni(P^{Me}{}_{2}N^{Ph}{}_{2})_2]^{2+}$, which has a much smaller substituent on P, is −54 kcal/mol [22,23]. Similarly, changing the substituents on N changes the pK_a values of the protonated pendent amines (or the proton acceptor abilities of the pendent amines, reaction 2 of Fig. 15). Using this approach, we have been able to tune the driving force for H_2 addition (ΔG°_{H2}) for $[Ni(P^{R}{}_{2}N^{R'}{}_{2})_2]^{2+}$ complexes over a range from −7.9 kcal/mol (R = Cy, R′ = *t*Bu) to +13.8 kcal/mol (R = Me, R′ = Ph) (Fig. 16) [22,23,43,46].

As expected, complexes with negative free energies for H_2 addition are found to be good H_2 oxidation catalysts, while complexes with positive values correspond to H_2 production catalysts (Fig. 16). We have studied two series of complexes in an effort to control the thermodynamic driving force for H_2 production catalysts. For one series, $[Ni(P^{Ph}{}_{2}N^{C6H4X}{}_{2})_2]^{2+}$ complexes, the para substituent of the benzene ring attached to the N atoms was varied from OMe to Br in an attempt to increase the acidity of the protonated pendent amine without changing the steric properties of the catalyst [22]. It was found that the turnover frequencies of these catalysts increased from 480 s^{-1} to 1040 s^{-1}, as the pK_a of the free amine corresponding to the pendant amine decreased from OMe (11.9) to Br (9.4) (Table 2). For a second series, $[Ni(P^{R}{}_{2}N^{Ph}{}_{2})_2]^{2+}$ complexes, the substituents on P were varied while the substituent on N remained constant (Table 3) [23,24]. As the hydride donor ability (the reverse of reaction 1 of Fig. 15) increased from R = Ph (ΔG°_{H-} = 59.0 kcal/mol) to R = Me (ΔG°_{H-} = 54 kcal/mol, where a smaller ΔG°_{H-} value indicates a better hydride donor), the turnover frequency of the catalyst for H_2 production using protonated dimethylformamide as the proton source in the presence of water, increased from 720 to 6700 s^{-1}. It was also found that R groups with bulky substituents on the second carbon atom result in decreased rates, attributed to steric interactions between the acid and substituents on the P atom as the acid approached the N atom in an endo position. Thus increasing the hydride donor ability of Ni increases the rate of H_2 production, but bulky substituents on P slow the reaction.

For the $Ni(P^{Ph}{}_{2}N^{C6H4X}{}_{2})_2]^{2+}$ series, the overpotenials are relatively constant as catalytic rates increase for X = OMe to Br (Table 2) [22,23], whereas the overpotentials increase as the catalytic rates increase for the $[Ni(P^{R}{}_{2}N^{Ph}{}_{2})_2]^{2+}$ complexes.(Table 3) This difference in behavior can be traced to the fact that hydride donor abilities increase as the redox potentials of the Ni(II/I) couple becomes more negative, but the acidity of the pendent amine increases as this redox potential becomes more positive. As a result, in wet acetonitrile solutions using protonated dimethylformamide as the acid (pK_a = 6.1), the fastest catalyst in the $Ni(P^{Ph}{}_{2}N^{C6H4X}{}_{2})_2]^{2+}$ series, $Ni(P^{Ph}{}_{2}N^{C6H4Br}{}_{2})_2]^{2+}$, has

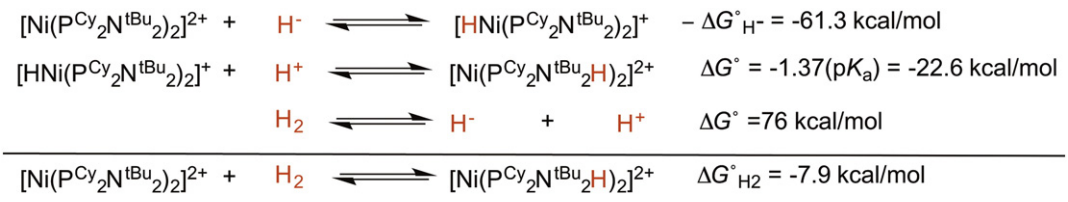

Fig. 15. Themochemical cycle for the calculation of the driving force for hydrogen addition.

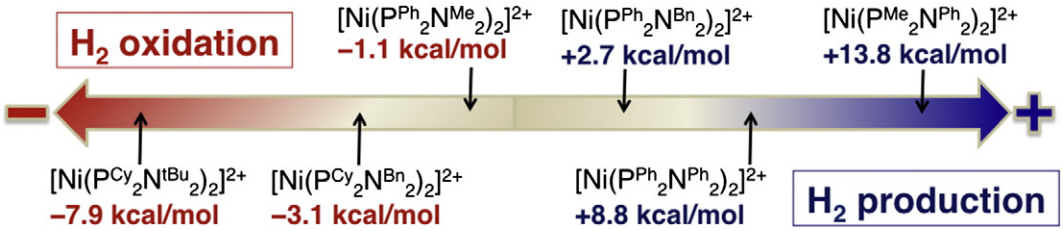

Fig. 16. Free energy of H_2 addition to $[Ni(P^R{}_2N^{R'}{}_2)_2]^{2+}$ catalysts, spanning a range of 21 kcal/mol.

a catalytic rate of 1040 s^{-1} with a modest overpotential of 290 mV, while for the $[Ni(P^R{}_2N^{Ph}{}_2)_2]^{2+}$ series, the fastest catalyst, $[Ni(P^{Me}{}_2N^{Ph}{}_2)_2]^{2+}$, has a catalytic rate of 6,700 s^{-1} but a much larger overpotential of 545 mV [58–60].

For H_2 oxidation catalysts, a series of $[Ni(P^{Cy}{}_2N^{R'}{}_2)_2]^{2+}$ complexes have been studied to determine the influence of the driving force for H_2 addition to form the corresponding $[Ni(P^{Cy}{}_2N^{R'}{}_2H)_2]^{2+}$ on the rate of catalytic H_2 oxidation. As expected, the rate of catalytic H_2 oxidation increases as ΔG°_{H2} becomes more negative as seen from the data shown in Table 4. For example, the rate of catalytic H_2 oxidation for $Ni(P^{Cy}{}_2N^{Bn\text{-}Ala\text{-}OMe}{}_2)_2]^{2+}$ (3.4 s^{-1} at 1.0 atm H_2 and 22 °C, $\Delta G^\circ_{H2} = -2.3$ kcal/mol) is less than that observed for $Ni(P^{Cy}{}_2N^{tBu}{}_2)_2]^{2+}$ (65 s^{-1} at 1.0 atm H_2 and 22 °C, $\Delta G^\circ_{H2} = -7.9$ kcal/mol) by a factor of 20 [33,46]. Reducing the pK_a, and thereby ΔG°_{H2}, resulted in a slower rate. While this is a general trend, there is some scatter in the data as the Bn–OMe complex is slightly slower than the Bn complex, despite a larger pK_a.

It is also possible to design catalysts with values of ΔG°_{H2} close to zero. These catalysts result in slower rates, but they also operate at much lower overpotentials. For example, $Ni(P^{Ph}{}_2N^{Bn}{}_2)_2]^{2+}$ ($\Delta G^\circ_{H2} = +2.7$ kcal/mol) exhibits a rate of 4 s^{-1} for H_2 production with an overpotential of 50 mV [54]. The potential at which catalysis occurs for this complex also depends on the pH of the solution, indicating that the potential of the catalyst is controlled by the degree of protonation of the catalyst in its oxidized and reduced forms. For the catalyst $[Ni(P^{Ph}{}_2N^{R}{}_2)_2]^{2+}$ (where R = $CH_2CH_2OCH_3$), for which $\Delta G^\circ_{H2} = +0.84$ kcal/mol, both catalytic H_2 production and oxidation are observed in the presences of a 1:1 buffered acid solution, i.e. this catalyst operates in both directions in a manner very similar to that of enzymes (Fig. 17) [45]. In addition, the rate of H_2 production is inhibited by the presence of H_2, as expected for a truly reversible system.

A plot of log[TOF] vs. ΔG°_{H2} for $[Ni(P^R{}_2N^{R'}{}_2)_2]^{2+}$ H_2 production catalysts that are not sterically encumbered at P is shown in Fig. 18. This plot is similar to a Tafel plot for catalytic reactions occurring at an electrode surface and suggests (using the equation in Fig. 18) a k_0 value of approximately 1 s^{-1} when the driving force for H_2 production/oxidation is 0.0 V ($\Delta G^\circ_{H2} = 0.0$ kcal/mol) and a rate of approximately 5 s^{-1} for this class of complexes at an overpotential of 100 mV ($\Delta G^\circ_{H2} = 2.3$ kcal/mol). Just as for surface species on an electrode surface, increasing the driving force for the H_2 production reaction by tuning the Ni(II/I) couple to more negative potentials (thereby increasing the hydride donor ability of $[HNi(P^R{}_2N^{R'}{}_2)_2]^+$) or increasing the acidity of the protonated pendent base will increase the overall catalytic rate regardless of the identity of the rate-determining step.

To summarize, the hydride donor/acceptor abilities of $[Ni(P^R{}_2N^{R'}{}_2)_2]^{2+}$ complexes can be controlled via a careful manipulation of the first coordination sphere. The pK_a values of the protonated pendent amines in the second coordination sphere can be controlled by varying the electron donor/withdrawing abilities of the substituent on N. This control can be used to design catalysts for H_2 production, H_2 oxidation, or catalysts that can operate in both directions.

Table 2
Turnover frequencies (TOF, s^{-1}) and overpotentials (OP, mV, in parentheses) for electrocatalytic hydrogen production by $[Ni(P^{Ph}{}_2N^{C6H4X}{}_2)_2]^{2+}$ complexes in pure CH_3CN (dry) and CH_3CN/H_2O (wet) solutions with $[(DMF)H]^+$ as the proton source. The pK_a listed corresponds to the free *p*-$XC_6H_4NH_3^+$ anilinium ion in CH_3CN.

X	Dry TOF (OP)	Wet TOF (OP)	pK_a
OMe	310 (310)	480 (330)	11.8
Me	590 (340)	770 (360)	11.2
$CH_2P(O)(OEt)_2$	500 (320)	1850 (370)	10.7
H	590 (300)	720 (320)	10.6
Br	740 (280)	1040 (290)	9.4
CF_3	95 (300)	120 (300)	8.0

Table 3
Turnover frequencies (TOF, s^{-1}) and overpotentials (OP, mV, in parentheses) for electrocatalytic hydrogen production by $[Ni(P^R{}_2N^{Ph}{}_2)_2]^{2+}$ complexes in pure CH_3CN (dry) and CH_3CN/H_2O (wet) solutions with $[(DMF)H]^+$ as the proton source. The ΔG°_{H2} listed corresponds to the calculated free energy of hydrogen addition to the metal complex.

R	TOF dry (OP)	TOF wet (OP)	ΔG°_{H2}
Methyl	1540 (500)	6700 (545)	13.8
n-butyl	46 (450)	1820 (500)	10.7
2-phenylethyl	31 (330)	1080 (450)	10.0
2,4,4-trimethylpentyl	<1 (360)	69 (450)	10.2
Benzyl	7 (410)	130 (460)	8.4

4.3. Designing catalysts to avoid 'pinched' isomers

As discussed above, the rate of catalysis for $[Ni(P^R{}_2N^{R'}{}_2)_2]^{2+}$ H_2 production catalysts is limited by the fact that the kinetically preferred **x/x** isomer formed upon protonation of the reduced Ni species cannot directly eliminate H_2. This isomer must undergo isomerization to form the **e/e** isomer, which can eliminate H_2. In an effort to avoid the formation of the 'exo' pinched protonated $[Ni(P^R{}_2N^{R'}{}_2H)_2]^{2+}$ complexes with an intraligand NH•••N bond (Fig. 19, A), a new catalyst, $[Ni(P^{Ph}{}_2N^{Ph})_2]^{2+}$ with one less N atom in each diphosphine ligand was designed [61]. Stabilization by a second N•••H interaction in an exo 'pinched' form of $[Ni(P^{Ph}{}_2N^{Ph})_2]^{2+}$ (Fig. 19, B) is not possible because of the lack of a second amine.

As expected, $[Ni(P^{Ph}{}_2N^{Ph})_2]^{2+}$ is an electrocatalyst for the reduction of protons in acetonitrile to produce hydrogen. However, unlike the previously discussed $[Ni(P^R{}_2N^{R'}{}_2)_2]^{2+}$ hydrogen production catalysts, the reactions are first order with respect to the catalyst and acid,

Table 4
Turnover frequencies and thermodynamic parameters for hydrogen oxidation catalysts of the form $Ni(P^{Cy}{}_2N^{R'}{}_2)_2^{2+}$. All of the reported data were collected using acetonitrile with added water as the solvent and triethylamine as the base.

R′	p$K_{a(protonated\text{-}amine)}$	ΔG_{H2}	TOF (s^{-1})
Bn-Ala-OMe	12.8	−2.3	3.4
Bn	13.4	−3.1	10
Bn-OMe	15.0	−3.6	7
^{t}Bu	16.5	−7.9	65

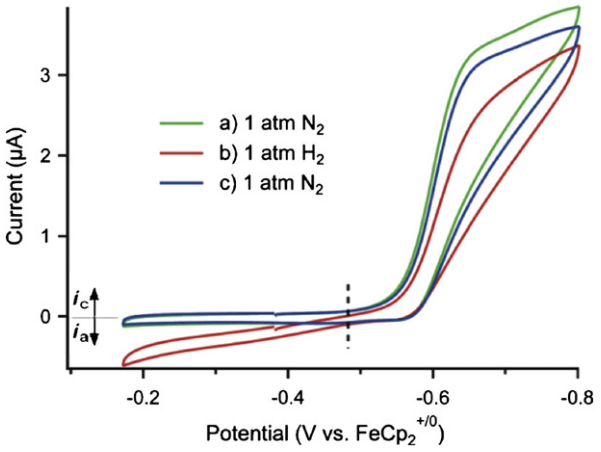

Fig. 17. The complex $[Ni(P^{Ph}{}_2N^{CH2CH2OCH3}{}_2)_2]^{2+}$ has a $\Delta G°_{H2}$ close to zero and is operates as both a hydrogen oxidation and a hydrogen production catalyst. Reprinted with permission from Smith, 2012, Wiley-VCH [45].

and an acid independent region was not achieved with this catalyst [61]. This catalyst has an extremely fast rate for hydrogen production with a turnover frequency of 33,000 s^{-1} (0.43 M $[H(DMF)]^+$). The addition of water resulted in an increase in the turnover frequency to 106,000 s^{-1} (0.43 M $[H(DMF)]^+$, 1.2 M H_2O), nearly two orders of magnitude faster than the analogous $[Ni(P^{Ph}{}_2N^{Ph}{}_2)_2]^{2+}$ derivative. Although the 'exo' pinched species has been eliminated in the design of this catalyst, the nitrogen can still be protonated in the exo position, requiring isomerization to the endo position for catalysis. The additional rate enhancement in the presence of water is attributed to the ability of water to facilitate endo protonation. Although the catalyst functions with a high overpotential (625 mV vs ~300 mV for the $[Ni(P^R{}_2N^{R'}{}_2)_2]^{2+}$ complexes), these results clearly indicate that properly designed pendent amine bases in the second coordination sphere functioning as proton relays are capable of promoting extremely fast H–H bond formation and proton transfer from solution to the metal center.

Considering the evolution of the Ni-pendent amine catalysts (Fig. 20), the improvements over the $[Ni(PNP)_2]^{2+}$ catalysts were achieved by incorporating the *positioned* pendent amine in the $[Ni(P^R{}_2N^{R'}{}_2)_2]^{2+}$ class of catalysts, which resulted in a dramatic enhancement in rates. However, the presence of intraligand NH•••N hydrogen bonding in these complexes also led to bottle necks in catalytic pathways for hydrogen production catalysis. The $[Ni(P^{Ph}{}_2N^{Ph})_2]^{2+}$ catalyst represents an attempt to avoid this intraligand hydrogen bonding, and higher catalytic activities are observed for this complex, but also with an increase in the overpotential. Overall, the progression of catalysts (Figs. 4 and 19) represents a significant evolution of the

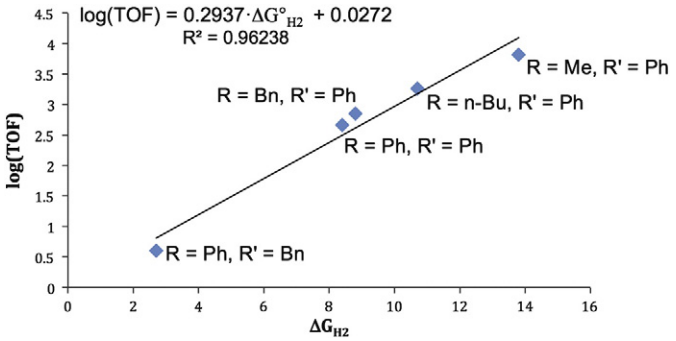

Fig. 18. Plot of log(TOF) for $[Ni(P^R{}_2N^{R'}{}_2)_2]^{2+}$ H_2 production catalysts vs. the driving force for H_2 elimination, $\Delta G°_{H2}$.

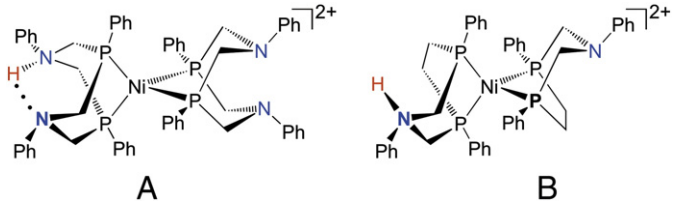

Fig. 19. Exo protonated (A) $[Ni(P^{Ph}{}_2N^{Ph})(P^{Ph}{}_2N^{Ph}H)]$ and (B) $[Ni(P^{Ph}{}_2N^{Ph})(P^{Ph}{}_2N^{Ph}H)]^{2+}$ catalysts.

structures of the first and second coordination spheres and in catalytic performance. Future challenges in the evolution of these catalysts will entail understanding and controlling the relationship between TOFs and overpotentials.

5. Contributions from the outer coordination sphere

The preceding discussions have focused primarily on the roles of the first and second coordination spheres in determining catalyst performance. It is clear that geometry and electron donor ability of the ligands in the first coordination sphere can be used to rationally introduce a coordination site for H_2 and hydride binding and to control the bias of the catalyst toward H_2 oxidation or production. The introduction of the pendent base in the second coordination sphere can dramatically increase catalytic rates by facilitating both the heterolytic cleavage and formation of the H–H bond, facilitating intra- and intermolecular proton transfer, and dramatically reducing overpotentials by coupling proton and electron transfer processes. In the discussions of the role of water it has also been evident that structural features not included in the first and second coordination spheres (i.e. the outer coordination sphere) can also play an important role in catalyst performance. In this section we summarize some of our results to date on the role of the outer coordination sphere.

5.1. Water

Control of proton movement *beyond* the second coordination sphere, as manifested in the proton conduction channels of the hydrogenase enzymes, constitutes a natural extension of our efforts to incorporate pendent bases/acids in the second coordination sphere. In nearly all of the above catalysts, water is observed to enhance catalysis, from 1.5 to 50 times. Catalytic studies as well as computational studies and NMR studies indicate that water facilitates isomerization by assisting proton transfer between the pendent amine in the second coordination sphere and a base in solution, [22] reducing the need for a bulky base to closely approach the metal center. In this role, water is

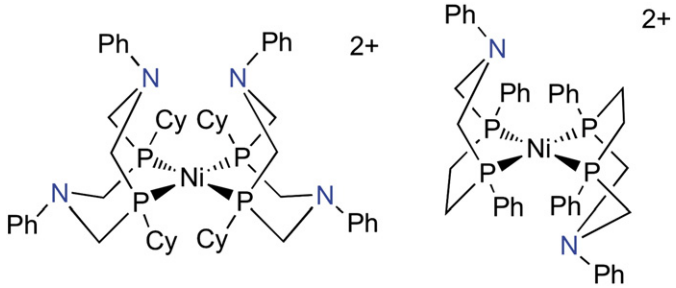

Fig. 20. The evolution of the second coordination sphere of the Ni-based hydrogen oxidation and production catalysts. Turnover frequencies and operating potentials are shown for hydrogen oxidation (top) and hydrogen production (bottom).

an active component of an outer coordination sphere, facilitating the overall catalytic reaction by reducing the barrier to intermolecular proton transfer. It is interesting to note that for some catalysts there is an optimal concentration of water as shown in Fig. 21, suggesting multiple roles for water, only some of which benefit catalysis.

5.2. Ionic liquids

In an effort to examine the possibility of using the solvent itself to deliver protons to the catalyst in a manner similar to that of the proton channels in the hydrogenase enzymes, the ionic liquid dibutylformamidium bis(trifluoromethanesulfonyl)amide ([(DBF)H]NTf_2) was selected as a solvent, and the $[Ni(P^{Ph}_2N^{Ph}_2)_2]^{2+}$ catalyst was modified so that the phenyl groups attached to N contained a hexyl group in the para position $[Ni(P^{Ph}_2N^{C6H4hexyl}_2)_2]^{2+}$ to enhance solubility. In this catalytic system the protic ionic liquid could serve as electrolyte, acid, and solvent, and the pK_a value of the ionic liquid (~6.1 in acetonitrile) closely matches that of the reduced catalyst. This catalytic system had a rate between 43,000 and 53,000 s^{-1}, with no increase in overpotential compared to acetonitrile, where the rate was only 740 s^{-1} (Fig. 22) [62,63]. This remarkable increase, nearly 50 times over the acetonitrile solution utilizing $[(DMF)H]^+$ as the acid, was suggested to be the result of an enhanced ability of the ionic liquid to deliver protons, with the hexyl tail playing an important role in organizing the acidic solvent and catalyst to enhance proton delivery. The essential role of the hydrophobic hexyl tail is suggested by the observation that other catalysts with less hydrophobic substituents on N were only moderately faster or even exhibited a decrease in rate compared to the same catalyst in acetonitrile. While this effect is not yet fully understood, the results provide evidence for an important role for the outer coordination sphere in the delivery of protons under the right set of conditions.

5.3. Amino acids and peptides

The water and ionic liquid discussed in the preceding paragraphs are not directly attached to the molecular catalyst and hence are not an integral part of the catalyst itself. In an attempt to integrate enzyme-like features into these $[Ni(P^R_2N^{R'}_2)_2]^{2+}$ catalysts, amino acids and dipeptides were attached to the $[Ni(P^{Ph}_2N^{Ph}_2)_2]^{2+}$ core via meta or para substituents of the N^{Ph} group.[32,64] A series of hydrophobic, hydrophilic, basic and acidic amino acids were used, both esterified on the side chain functional group and C-terminus, as well as in their unprotected

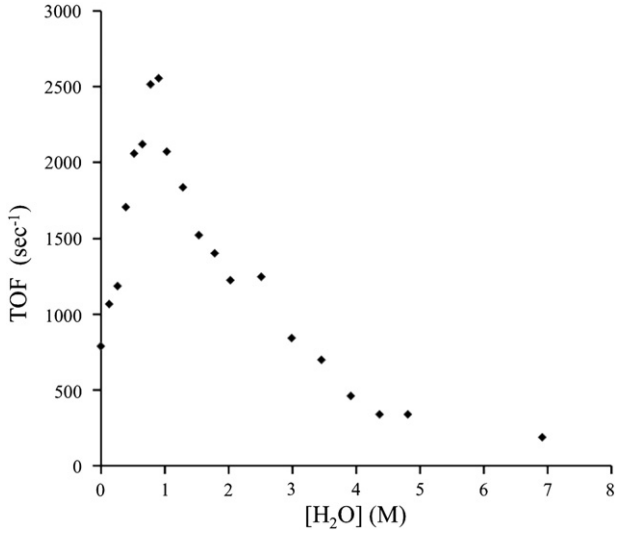

Fig. 21. Hydrogen production turnover frequency (s^{-1}) of $[Ni(P^{Ph}_2N^{NNA\text{-}Lys(Boc)OMe}_2)_2]^{2+}$ as a function of water concentration. Initially water enhances the rate of catalysis, but after the maximum concentration is reached, further additions of water decrease the rate dramatically.

forms. The rates of the resulting complexes are shown in Table 5 and several interesting insights have come from these data. All of the catalysts are active for hydrogen production, with their rates ranging over an order of magnitude, both slower than and faster than the unmodified $[Ni(P^{Ph}_2N^{Ph}_2)_2]^{2+}$ parent catalyst. Hydrophobic, alcoholic, ester and aromatic functional groups neither enhance nor promote catalysis, while amide bonds, acidic functional groups, and basic functional groups increasingly enhance catalysis.

This data, aided by molecular dynamics simulations, suggest that the amide, acid and basic groups may enhance catalysis by increasing the concentration of the substrates around the active site or by facilitating proton movement. That polar substituents do not enhance catalysis is interesting and suggests that the dielectric around the active site is not important for molecular catalysts, a function that has been suggested as important for enzymatic catalysts [34,65]. Larger substituents do not decrease the catalytic rate, as the larger catalysts are also the fastest. However, in the *para*-substituted complexes, electron transfer is slower, resulting in the requirement of a higher overpotential to achieve their fastest rates. Substitution of the complexes in the *meta* position resulted in overpotentials comparable to the parent complex, an observation that was explained by the more compact nature of the *meta*-substituted complexes based on MD simulations [64]. A more compact structure may allow more facile structural rearrangements reducing the barrier for the square planar to tetrahedral structural rearrangement that occurs upon reduction of these catalysts. Alternatively, a smaller more compact structure will also facilitate a closer approach of the catalyst to the electrode and decrease the barrier for electron transfer.

A key observation from this work is the need for precise positioning. The amino acids and dipeptides are constrained only at the pendent amine and otherwise cover a very large conformational space [64]. This is shown in Fig. 23 where the structures along the molecular dynamics trajectory of the *p*-NNA-SerOMe (defined in Table 5) complex are overlaid to show the conformational flexibility of the dipeptide substituent. The result of this flexibility is that global outer coordination sphere features, such as concentrating water and protons or altering the overall dielectric, can be integrated into the catalyst. But introducing specific local features, such as a hydrogen bond or creating a well-defined polar pocket, is not possible. The weak interactions and stabilizations used so well by enzymes to create these local features are still absent. Complexes with stable secondary and tertiary structures will be needed to achieve precise placement of functional groups in the outer coordination sphere in a manner analogous to the positioning of the pendent amine in the second coordination sphere. If achieved, a well-structured outer coordination sphere has the potential to control proton movement, influence electron transfer rates and overpotentials, and influence reactivity via dynamics, as discussed in more detail in the challenges section.

5.4. Binding to electrodes

For practical use of molecular electrocatalysts in fuel cells, one option would be to attach them to a surface. Efforts in this direction have been reported for attaching the $[Ni(P^R_2N^{R'}_2)_2]^{2+}$ derivatives to indium tin oxide/multiwalled carbon nanotube (ITO/MWCNT) surfaces via covalent attachment through a carboxyl group or π–π stacking using a pyrene derivative [66,67]. In both cases, the surface immobilized catalysts were active for both hydrogen production and oxidation, though only moderate to slow rates (~5 s^{-1} and ~1 s^{-1}, respectively) were reported. One of the pyrene derivatives exhibited an attractive current density of 200 $mA/cm^{-2}/mg_{cat}$, a promising advancement. The catalyst stability on the surface was tested and appeared to be nearly quantitatively stable for the 10 h over which it was tested.

A thiophene derivative was used in a separate approach to allow polymerization to a glassy carbon surface. In this case, no current enhancement was observed for the immobilized catalyst. This could be due to an inability of the catalyst to undergo structural rearrangements

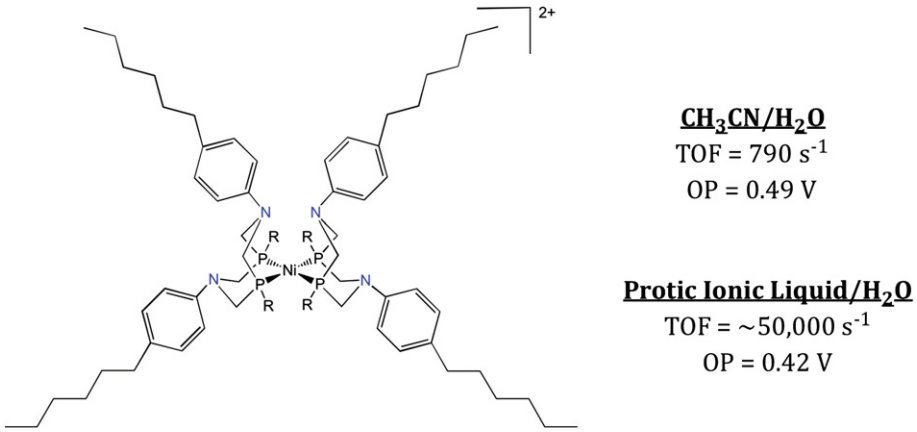

Fig. 22. Overpotential and TOF of $[Ni(P^{Ph}{}_2N^{C6H4hexyl}{}_2)_2]^{2+}$ in ionic liquid and CH_3CN.

upon reduction, which could be brought about by the four thiophene functional groups restricting motion. This may suggest that the tether to the catalyst is too short. It is also possible that the catalyst is damaged during oxidation to create the polymer film. The presence of function for the ITO/MWCNT immobilized catalyst, which also has the potential to bind all four sites to the surface, makes it difficult to determine precisely what is different about the two catalyst/surface systems. In both cases, the activity is severely reduced or not observed, highlighting the challenges to success with these types of surface attachments. As with other mechanistic aspects of these catalysts, one approach to limit potential problems is to reduce the number of pendent amines, lowering the possibility for restricting structural rearrangements. Additionally, lengthening the tether may also allow more structural freedom. Efforts to understand what is happening at the surface so the catalysts can be optimized are underway.

Table 5
Rates of amino acid and dipeptide substituted $Ni(P_2N_2)_2$ catalysts, with the substituent off of the p-position of the N-Phenyl ring. Naming consists of three parts: substitution position (p = para), the non-natural amino acid linker 4-(4-aminophenyl propionic acid) (NNA), and the three letter shorthand for the amino acid (i.e. Ser), if appropriate, or the terminating group (i.e. NH_2 or OCH_3).

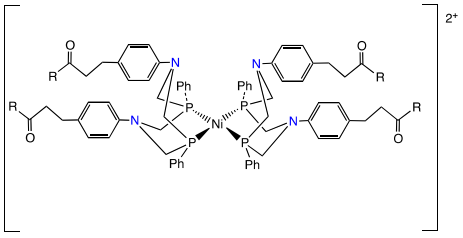

$[Ni(P^{Ph}{}_2N^{NNA\text{-}amino\ acid/ester}{}_2)]^{2+}$	Wet TOF, OP ~ 420 mV
*p*NNA-Lys	3350
*p*NNA-Glu	3100
*p*NNA-Asp	2600
*p*NNA-Ala	2600
*p*NNA-Lys(Boc)OMe	2000
*p*NNA-GlyOEt*	1750
p-NNA-TyrOMe	1200
*p*NNA-Asp(OMe)OMe	1150
p-NNA-AlaOEt	1100
p-NNA-SerOMe	1100
*p*NNA-AlaOEt	1080
p-NN-NH_2	1030
*P*nna	970
p-NN-OEt	950
p-NNA-PheOMe	910
*p*NNA-Glu(OMe)OMe	900
*p*NNA-Gly	570
*p*NNA-NN-OEt	250
$[Ni(P^{Ph}{}_2N^{Ph}{}_2)_2]^{2+}$	720 (OP 320 mV)

6. Summary

The results discussed above highlight the substantial promise that designed molecular catalysts hold for the electrocatalytic production and oxidation of hydrogen. The first, second, and outer coordination spheres of $[Ni(P^{R}{}_2N^{R'}{}_2)_2]^{2+}$ complexes all play important roles in determining the overall performance of these H_2 production and oxidation catalysts. The first coordination sphere can be used to rationally introduce a coordination site for substrate binding and to control the bias of the catalyst toward either H_2 oxidation or production. The introduction of a pendent amine in the second coordination sphere can dramatically increase the catalytic rates by facilitating both the heterolytic cleavage and formation of the H–H bond. Because formation of H_2 complexes for these Ni catalysts is unfavorable, positioning the pendent amines is critical for achieving high rates of H–H bond cleavage/formation. The pendent amines also play important roles in intra- and intermolecular proton transfer, and dramatically reduce overpotentials by introducing physical pathways that lead to the coupling of proton and electron transfer steps. The outer coordination sphere has been demonstrated to enhance rates and affect overpotentials, in some cases dramatically, emphasizing the importance of its inclusion in a well-designed catalyst.

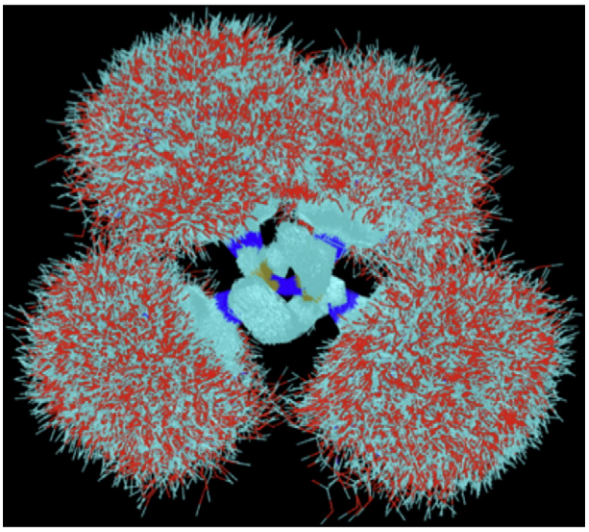

Fig. 23. The $Ni(P_2N_2)_2$ with the NNA-SerOMe dipeptide attached. The dipeptides in these complexes are not constrained and cover a large conformational space. This demonstrates the need for the precise positioning achieved by a structured scaffold to introduce specific, rather than global, features into molecular catalysts.

The ultimate goal of catalyst design is to have a sufficiently developed model of catalysis so that catalyst performance under a selected set of conditions can be predicted. This would enable researchers to select the optimal catalysts for a given application. Such an optimal catalyst might need to run in strongly acidic or basic conditions, incorporate an inexpensive metal, and have a certain combination of overpotential and rate. Of course once such a catalyst has been chosen, it must be possible to synthesize the designed catalyst, and this can be a challenging task. For the $[Ni(P^{R}_2N^{R'}_2)_2]^{2+}$ catalyst reported here, it is now possible to accurately predict the pK_a values, hydride donor abilities, and homolytic bond dissociation free energies from a knowledge of the Ni(II/I) and Ni(I/0) couples of the corresponding $[Ni(diphosphine)_2]^{2+}$ complexes [8]. This allows the relative free energies of all of the possible intermediates for the catalytic oxidation/production of H_2 to be predicted under any specific set of conditions. The ability to determine the relative free energies of all of the intermediates results in the ability to optimize the catalytic process as a whole rather than for just an individual step. This represents a significant advance in our ability to design the first coordination sphere of $[Ni(diphosphine)_2]^{2+}$ catalysts.

However, models do not currently exist that properly account for the interactions between the first and second coordination spheres for catalysts containing pendent bases and acids in the second coordination sphere. This ability to predict the pK_a values of the pendent amine in different oxidation states and the influence of the pendent amine on parameters such as hydride donor abilities, redox potentials, and pK_a values of hydride ligands for catalysts possessing acidic or basic groups in the second coordination sphere is needed before a comprehensive model can be developed for complex catalysts containing an active second coordination sphere. Additionally, our understanding of the outer coordination sphere is rudimentary and greater structural control of this coordination sphere is needed to achieve more precisely designed functionality. Work is in progress to achieve these goals.

The ability to control the movement of protons in synthetic catalysts with the same degree of precision as manifested in enzymes is still not possible. As discussed above, much has been learned about proton movement in $[Ni(P^{R}_2N^{R'}_2H)_2]^{2+}$complexes including intra- and intermolecular proton exchange and PCET reactions. However, the selective delivery and removal of protons to or from endo positions in these catalysts has not been achieved and remains a major challenge to achieving the optimal performance for this class of catalysts that may ultimately rival or exceed that of the hydrogenase enzymes. Achieving this goal may require new and more sophisticated types of relays and new classes of complexes, and the coupling of all three coordination spheres in a rational design.

The high sensitivity of catalytic rates to the incorporation and arrangement of pendent amines in the ligand and their multiple roles during the catalytic oxidation and production of H_2 suggests that proton relays may be important for developing H_2 oxidation and production catalysts based on other metals. Progress has been made in this area for both Co and Fe catalysts [29,48]. In addition, pendent bases and acids in the second coordination sphere appear to be critical participants in other important multi-proton, multi-electron catalytic reactions such as the reduction of oxygen [68–71], water oxidation, CO_2 reduction [19], formate oxidation [56], etc. for both enzymes and molecular catalysts. An understanding of how to precisely construct the geometrical pathways in the outer coordination sphere required for proton movement between the solution and the metal with the ultimate formation or cleavage of bonds to hydrogen and the ability to control the energetics of the multiple steps involved in these processes will be required for the rational design of molecular catalysts for the wide range of energy storage and utilization reactions necessary for a secure energy future.

Acknowledgements

MLH and DLD acknowledge the support of the Center for Molecular Electrocatalysis, an Energy Frontier Research Center funded by the US Department of Energy, Office of Science, Office of Basic Energy Sciences. WJS acknowledges the support of the DOE Office of Science Early Career Research Program through the Office of Basic Energy Sciences. Pacific Northwest National Laboratory is operated by Battelle for the U.S. Department of Energy.

References

[1] R.M. Bullock, Catalysis Without Precious Metals, 1st ed. Wiley-VCH, 2010.
[2] S.S. Ott, M.M. Kritikos, B.B. Akermark, L.L. Sun, R.R. Lomoth, A biomimetic pathway for hydrogen evolution from a model of the iron hydrogenase active site, Angew. Chem. Int. Ed. 43 (2004) 1006–1009.
[3] L. Schwartz, J. Ekström, R. Lomoth, S. Ott, Dynamic ligation at the first amine-coordinated iron hydrogenase active site mimic, Chem. Commun. (2006) 4206–4208.
[4] L.L. Schwartz, G.G. Eilers, L.L. Eriksson, A.A. Gogoll, R.R. Lomoth, S.S. Ott, Iron hydrogenase active site mimic holding a proton and a hydride, Chem. Commun. (2006) 520–522.
[5] S.S. Jiang, J.J. Liu, Y.Y. Shi, Z.Z. Wang, B.B. Akermark, L.L. Sun, Fe–S complexes containing five-membered heterocycles: novel models for the active site of hydrogenases with unusual low reduction potential, Dalton Trans. (2007) 896–902.
[6] M. Wang, L. Chen, X. Li, L. Sun, Approaches to efficient molecular catalyst systems for photochemical H2 production using [FeFe]-hydrogenase active site mimics, Dalton Trans. 40 (2011) 12793–12800.
[7] L. Chen, M. Wang, F. Gloaguen, D. Zheng, P. Zhang, L. Sun, Multielectron-transfer templates via consecutive two-electron transformations: iron–sulfur complexes relevant to biological enzymes, Chem. Eur. J. 18 (2012) 13968–13973.
[8] S. Chen, R. Rousseau, S. Raugei, M. Dupuis, D.L. DuBois, R.M. Bullock, Comprehensive thermodynamics of nickel hydride bis(diphosphine) complexes: a predictive model through computations, Organometallics 30 (2011) 6108–6118.
[9] D.M. Heinekey, Hydrogenase enzymes: recent structural studies and active site models, J. Organomet. Chem. 694 (2009) 2671–2680.
[10] C. Tard, C.J. Pickett, Structural and functional analogues of the active sites of the [Fe]-, [NiFe]-, and [FeFe]-hydrogenases, Chem. Rev. 109 (2009) 2245–2274.
[11] F. Gloaguen, T.B. Rauchfuss, Small molecule mimics of hydrogenases: hydrides and redox, Chem. Soc. Rev. 38 (2009) 100–108.
[12] J.-F. Capon, F. Gloaguen, F.Y. Petillon, P. Schollhammer, J. Talarmin, Organometallic diiron complex chemistry related to the $[2Fe]_H$ Subsite of $[FeFe]H_2$ase, Eur. J. Inorg. Chem. (2008) 4671–4681.
[13] D.J. Evans, C.J. Pickett, Chemistry and the hydrogenases, Chem. Soc. Rev. 32 (2003) 268–275.
[14] B.E. Barton, M.T. Olsen, T.B. Rauchfuss, Aza- and oxadithiolates are probable proton relays in functional models for the [FeFe]-hydrogenases, J. Am. Chem. Soc. 130 (2008) 16834–16835.
[15] J.I. van der Vlugt, T.B. Rauchfuss, C.M. Whaley, S.R. Wilson, Characterization of a diferrous terminal hydride mechanistically relevant to the Fe-only hydrogenases, J. Am. Chem. Soc. 127 (2005) 16012–16013.
[16] J.D. Lawrence, H. Li, T.B. Rauchfuss, M. Bénard, M.-M. Rohmer, Diiron azadithiolates as models for the iron-only hydrogenase active site: synthesis, structure, and stereoelectronics, Angew. Chem. Int. Ed. 40 (2001) 1768–1771.
[17] D.L. DuBois, R.M. Bullock, Molecular electrocatalysts for the oxidation of hydrogen and the production of hydrogen — the role of pendent amines as proton relays, Eur. J. Inorg. Chem. (2011) 1017–1027.
[18] M. Rakowski DuBois, D.L. DuBois, The roles of the first and second coordination spheres in the design of molecular catalysts for H_2 production and oxidation, Chem. Soc. Rev. 38 (2009) 62–72.
[19] M. Rakowski DuBois, D.L. DuBois, Development of molecular electrocatalysts for CO_2 reduction and H_2 production/oxidation, Acc. Chem. Res. 42 (2009) 1974–1982.
[20] A.D. Wilson, R.H. Newell, M.J. McNevin, J.T. Muckerman, M. Rakowski DuBois, D.L. DuBois, Hydrogen oxidation and production using nickel-based molecular catalysts with positioned proton relays, J. Am. Chem. Soc. 128 (2006) 358–366.
[21] A.D. Wilson, R.K. Shoemaker, A. Miedaner, J.T. Muckerman, D.L. DuBois, M. Rakowski DuBois, Nature of hydrogen interactions with Ni(II) complexes containing cyclic phosphine ligands with pendent nitrogen bases, Proc. Natl. Acad. Sci. 104 (2007) 6951–6956.
[22] U.J. Kilgore, J.A.S. Roberts, D.H. Pool, A.M. Appel, M.P. Stewart, M. Rakowski DuBois, W.G. Dougherty, W.S. Kassel, R.M. Bullock, D.L. DuBois, $[Ni(P^{Ph}_2N^{C6H4X}_2)_2]^{2+}$ complexes as electrocatalysts for H_2 production: effect of substituents, acids, and water on catalytic rates, J. Am. Chem. Soc. 133 (2011) 5861–5872.
[23] U.J. Kilgore, M.P. Stewart, M.L. Helm, W.G. Dougherty, W.S. Kassel, M. Rakowski DuBois, D.L. DuBois, R.M. Bullock, Studies of a series of $[Ni(P^{R}_2N^{Ph}_2)_2(CH_3CN)]^{2+}$ complexes as electrocatalysts for H_2 production: substituent variation at the phosphorus atom of the P_2N_2 ligand, Inorg. Chem. 50 (2011) 10908–10918.
[24] S. Wiese, U.J. Kilgore, D.L. DuBois, R.M. Bullock, $[Ni(P^{Me}_2N^{Ph}_2)_2](BF_4)_2$ as an electrocatalyst for H_2 production, ACS Catal. 2 (2012) 720–727.
[25] V. Artero, M. Fontecave, Some general principles for designing electrocatalysts with hydrogenase activity, Coord. Chem. Rev. 249 (2005) 1518–1535.
[26] P.-A. Jacques, V. Artero, J. Pecaut, M. Fontecave, Cobalt and nickel diimine-dioxime complexes as molecular electrocatalysts for hydrogen evolution with low overvoltages, Proc. Natl. Acad. Sci. 106 (2009) 20627–20632.
[27] X. Hu, B.S. Brunschwig, J.C. Peters, Electrocatalytic hydrogen evolution at low overpotentials by cobalt macrocyclic glyoxime and tetraimine complexes, J. Am. Chem. Soc. 129 (2007) 8988–8998.
[28] J.L. Dempsey, B.S. Brunschwig, J.R. Winkler, H.B. Gray, Hydrogen evolution catalyzed by cobaloximes, Acc. Chem. Res. 42 (2009) 1995–2004.

[29] T.T. Liu, S.S. Chen, M.J. O'Hagan, M. Rakowski DuBois, R.M. Bullock, D.L. DuBois, Synthesis, characterization, and reactivity of Fe complexes containing cyclic diazadiphosphine ligands: the role of the pendent base in heterolytic cleavage of H_2, J. Am. Chem. Soc. 134 (2012) 6257–6272.

[30] D.H. Pool, D.L. DuBois, $[Ni(P^{Ph}_2N^{Ar}_2)_2(NCMe)][BF_4]_2$ as an electrocatalyst for H_2 production: $P^{Ph}_2N^{Ar}_2$ = 1,5-(di(4-(thiophene-3-yl)phenyl)-3,7-diphenyl-1,5-diaza-3, 7-diphosphacyclooctane), J. Organomet. Chem. 694 (2009) 2858–2865.

[31] A. Jain, S. Lense, J.C. Linehan, S. Raugei, H. Cho, D.L. DuBois, W.J. Shaw, Incorporating Peptides in the Outer-Coordination Sphere of Bioinspired Electrocatalysts for Hydrogen Production, Inorg. Chem. 50 (2011) 4073–4085.

[32] A. Jain, M.L. Reback, M.L. Lindstrom, C.E. Thogerson, M.L. Helm, A.M. Appel, W.J. Shaw, Investigating the role of the outer-coordination sphere in $[Ni(P^{Ph}_2N^{Ph\text{-}R}_2)_2]^{2+}$ hydrogenase mimics, Inorg. Chem. 51 (2012) 6592–6602.

[33] S. Lense, M.-H. Ho, S. Chen, A. Jain, S. Raugei, J.C. Linehan, J.A.S. Roberts, A.M. Appel, W. Shaw, Incorporating amino acid esters into catalysts for hydrogen oxidation: steric and electronic effects and the role of water as a base, Organometallics 31 (2012) 6719–6731.

[34] S. Karlin, Z.-Y. Zhu, K.D. Karlin, The extended environment of mononuclear metal centers in protein structures, Proc. Natl. Acad. Sci. 94 (1997) 14225–14230.

[35] D.E. Berning, A. Miedaner, C.J. Curtis, B.C. Noll, M. Rakowski DuBois, D.L. DuBois, Free-energy relationships between the proton and hydride donor abilities of $[HNi(diphosphine)_2]^+$ complexes and the half-wave potentials of their conjugate bases, Organometallics 20 (2001) 1832–1839.

[36] J.W. Raebiger, A. Miedaner, C.J. Curtis, S.M. Miller, O.P. Anderson, D.L. DuBois, Using ligand bite angles to control the hydricity of palladium diphosphine complexes, J. Am. Chem. Soc. 126 (2004) 5502–5514.

[37] C.J. Curtis, A. Miedaner, R. Ciancanelli, W.W. Ellis, B.C. Noll, M. Rakowski DuBois, D.L. DuBois, $[Ni(Et_2PCH_2NMeCH_2PEt_2)_2]^{2+}$ as a functional model for hydrogenases, Inorg. Chem. 42 (2003) 216–227.

[38] Y. Nicolet, C. Piras, P. Legrand, C.E. Hatchikian, J.C. Fontecilla-Camps, Desulfovibrio desulfuricans iron hydrogenase: the structure shows unusual coordination to an active site Fe binuclear center, Structure 7 (1999) 13–23.

[39] Y. Nicolet, A.L. de Lacey, X. Vernède, V.M. Fernandez, E.C. Hatchikian, J.C. Fontecilla-Camps, Crystallographic and FTIR spectroscopic evidence of changes in Fe coordination upon reduction of the active site of the Fe-only hydrogenase from desulfovibriodesulfuricans, J. Am. Chem. Soc. 123 (2001) 1596–1601.

[40] A. Silakov, B. Wenk, E. Reijerse, W. Lubitz, ^{14}N HYSCORE investigation of the H-cluster of [FeFe] hydrogenase: evidence for a nitrogen in the dithiol bridge, Phys. Chem. Chem. Phys. 11 (2009) 6592–6599.

[41] J.W. Peters, W.N. Lanzilotta, B.J. Lemon, L.C. Seefeldt, X-ray crystal structure of the Fe-only hydrogenase (CpI) from Clostridium pasteurianum to 18 angstrom resolution, Science 282 (1998) 1853–1858.

[42] S. Raugei, S. Chen, M.-H. Ho, B. Ginovska-Pangovska, R.J. Rousseau, M. Dupuis, D.L. DuBois, R.M. Bullock, The role of pendent amines in the breaking and forming of molecular hydrogen catalyzed by nickel complexes, Chem. Eur. J. (2012) 6493–6506.

[43] J.Y. Yang, R.M. Bullock, W.J. Shaw, B. Twamley, K. Fraze, M. Rakowski DuBois, D.L. DuBois, Mechanistic insights into catalytic H_2 oxidation by Ni complexes containing a diphosphine ligand with a positioned amine Base, J. Am. Chem. Soc. 131 (2009) 5935–5945.

[44] M. O'Hagan, W.J. Shaw, S. Raugei, S. Chen, J.Y. Yang, U.J. Kilgore, D.L. DuBois, R.M. Bullock, Moving protons with pendent amines: proton mobility in a nickel catalyst for oxidation of hydrogen, J. Am. Chem. Soc. 133 (2011) 14301–14312.

[45] S.E. Smith, J.Y. Yang, D.L. DuBois, R.M. Bullock, Reversible electrocatalytic production and oxidation of hydrogen at low overpotentials by a functional hydrogenase mimic, Angew. Chem. Int. Ed. 51 (2012) 3152–3155.

[46] J.Y. Yang, S. Chen, W.G. Dougherty, W.S. Kassel, R.M. Bullock, D.L. DuBois, S. Raugei, R. Rousseau, M. Dupuis, M. Rakowski DuBois, Hydrogen oxidation catalysis by a nickel diphosphine complex with pendent *tert*-butyl amines, Chem. Commun. 46 (2010) 8618–8620.

[47] M. O'Hagan, M.-H. Ho, J.Y. Yang, A.M. Appel, M. Rakowski DuBois, S. Raugei, W.J. Shaw, D.L. DuBois, R.M. Bullock, Proton Delivery and Removal in $[Ni(PR_2NR'_2)_2]^{2+}$ Hydrogen Production and Oxidation Catalysts, J. Am. Chem. Soc. 134 (2012) 19409–19424.

[48] E.S. Wiedner, J.Y. Yang, W.G. Dougherty, W.S. Kassel, R.M. Bullock, M. Rakowski DuBois, D.L. DuBois, Comparison of cobalt and nickel complexes with sterically demanding cyclic diphosphine ligands: electrocatalytic H_2 production by $[Co(P^{tBu}_2N^{Ph}_2)(CH_3CN)_3](BF_4)_2$, Organometallics 29 (2010) 5390–5401.

[49] E.S. Wiedner, J.Y. Yang, S. Chen, S. Raugei, W.G. Dougherty, W.S. Kassel, M.L. Helm, R.M. Bullock, M. Rakowski DuBois, D.L. DuBois, Stabilization of nickel complexes with Ni 0···H–N bonding interactions using sterically demanding cyclicdiphosphine ligands, Organometallics 31 (2012) 144–156.

[50] L.E. Fernandez, S. Horvath, S. Hammes-Schiffer, Theoretical analysis of the sequential proton-coupled electron transfer mechanisms for H_2 oxidation and production pathways catalyzed by nickel molecular electrocatalysts, J. Phys. Chem. C 116 (2012) 3171–3180.

[51] S. Horvath, L.E. Fernandez, A.V. Soudackov, S. Hammes-Schiffer, Insights into proton-coupled electron transfer mechanisms of electrocatalytic H_2 oxidation and production, Proc. Natl. Acad. Sci. 109 (2012) 15663–15668.

[52] L.E. Fernandez, S. Horvath, S. Hammes-Schiffer, Theoretical analysis of molecular electrocatalysts with flexible pendent amines for hydrogen production and oxidation, J. Phys. Chem. Lett. (submitted for publication).

[53] A.D. Wilson, K. Fraze, B. Twamley, S.M. Miller, D.L. DuBois, M. Rakowski DuBois, The role of the second coordination sphere of $[Ni(P^{Cy}_2N^{Bz}_2)_2](BF_4)_2$ in reversible carbon monoxide binding, J. Am. Chem. Soc. 130 (2008) 1061–1068.

[54] A.M. Appel, D.H. Pool, M. O'Hagan, W.J. Shaw, J.Y. Yang, M. Rakowski DuBois, D.L. DuBois, R.M. Bullock, $[Ni(P^{Ph}_2N^{Bn}_2)_2(CH_3CN)]^{2+}$ as an electrocatalyst for H_2 production: dependence on acid strength and isomer distribution, ACS Catal. 1 (2011) 777–785.

[55] K. Fraze, A.D. Wilson, A.M. Appel, M. Rakowski DuBois, D.L. DuBois, Thermodynamic properties of the Ni – H bond in complexes of the type $[HNi(P^R_2N^{R'}_2)_2](BF_4)$ and evaluation of factors that control catalytic activity for hydrogen oxidation/production, Organometallics 26 (2007) 3918–3924.

[56] B.R. Galan, J. Schöffel, J.C. Linehan, C. Seu, A.M. Appel, J.A.S. Roberts, M.L. Helm, U.J. Kilgore, J.Y. Yang, D.L. DuBois, C.P. Kubiak, Electrocatalytic oxidation of formate by $[Ni(P^R_2N^{R'}_2)_2(CH_3CN)]^{2+}$ complexes, J. Am. Chem. Soc. 133 (2011) 12767–12779.

[57] D.D.M. Wayner, V.D. Parker, Bond energies in solution from electrode potentials and thermochemical cycles. A simplified and general approach, Acc. Chem. Res. 26 (1993) 287–294.

[58] G.A.N. Felton, R.S. Glass, D.L. Lichtenberger, D.H. Evans, Iron-only hydrogenase mimics thermodynamic aspects of the use of electrochemistry to evaluate catalytic efficiency for hydrogen generation, Inorg. Chem. 45 (2006) 9181–9184.

[59] F.A. Armstrong, J. Hirst, Reversibility and efficiency in electrocatalytic energy conversion and lessons from enzymes, Proc. Natl. Acad. Sci. 108 (2011) 14049–14054.

[60] V. Fourmond, P.-A. Jacques, M. Fontecave, V. Artero, H2 evolution and molecular electrocatalysts: determination of overpotentials and effect of homoconjugation, Inorg. Chem. 49 (2012) 10338–10347.

[61] M.L. Helm, M.P. Stewart, R.M. Bullock, M. Rakowski DuBois, D.L. DuBois, A synthetic nickel electrocatalyst with a turnover frequency above 100,000 s^{-1} for H_2 production, Science 333 (2011) 863–866.

[62] J.A.S. Roberts, R.M. Bullock, Direct determination of equilibrium potentials for hydrogen oxidation/production by open circuit potential measurements in acetonitrile, Inorg. Chem. (submitted for publication).

[63] D.H. Pool, M.P. Stewart, M. O'Hagan, W.J. Shaw, J.A.S. Roberts, R.M. Bullock, D.L. DuBois, Acidic ionic liquid/water solution as both medium and proton source for electrocatalytic H_2 evolution by $[Ni(P_2N_2)_2]^{2+}$ complexes, Proc. Natl. Acad. Sci. 109 (2012) 15634–15639.

[64] M.L. Reback, B. Ginovska-Pangovska, M.-H. Ho, A. Jain, T.C. Squier, S. Raugei, J.A.S. Roberts, W.J. Shaw, The role of a dipeptide outer-coordination sphere on H2-production catalysts: influence on catalytic rates and electron transfer, Chem. Eur. J. (2012), http://dx.doi.org/10.1002/chem.201202849.

[65] R. Wolfenden, M.J. Snider, The depth of chemical time and the power of enzymes as catalysts, Acc. Chem. Res. 34 (2001) 938–945.

[66] A. Le Goff, V. Artero, B. Jousselme, P.D. Tran, N. Guillet, R. Métayé, A. Fihri, S. Palacin, M. Fontecave, From hydrogenases to noble metal–free catalytic nanomaterials for H_2 production and uptake, Science 326 (2009) 1384–1387.

[67] P.D. Tran, A. Le Goff, J. Heidkamp, B. Jousselme, N. Guillet, S. Palacin, H. Dau, M. Fontecave, V. Artero, Noncovalent modification of carbon nanotubes with pyrene-functionalized nickel complexes: carbon monoxide tolerant catalysts for hydrogen evolution and uptake, Angew. Chem. Int. Ed. 50 (2011) 1371–1374.

[68] T.A. Tronic, M. Rakowski DuBois, W. Kaminsky, M.K. Coggins, T. Liu, J.M. Mayer, Directing protons to the dioxygen ligand of a ruthenium(II) complex with pendent amines in the second coordination sphere, Angew. Chem. Int. Ed. 50 (2011) 10936–10939.

[69] T.A. Tronic, W. Kaminsky, M.K. Coggins, J.M. Mayer, Synthesis, protonation, and reduction of ruthenium–peroxo complexes with pendent nitrogen bases, Inorg. Chem. 51 (2012) 10916–10928.

[70] B.D. Matson, C.T. Carver, A. Von Ruden, J.Y. Yang, S. Raugei, J.M. Mayer, Distant protonated pyridine groups in water-soluble iron porphyrin electrocatalysts promote selective oxygen reduction to water, Chem. Commun. 48 (2012) 11100–11102.

[71] C.T. Carver, B.D. Matson, J.M. Mayer, Electrocatalytic oxygen reduction by iron tetra-arylporphyrins bearing pendent proton relays, J. Am. Chem. Soc. 134 (2012) 5444–5447.